



universität
wien

MASTERARBEIT

Titel der Masterarbeit

„Structure of Ultrathin Amorphous Carbon Films“

verfasst von

David Lindner, BSc

angestrebter akademischer Grad

Master of Science (MSc)

Wien, 2015

Studienkennzahl lt. Studienblatt:

A 066 876

Studienrichtung lt. Studienblatt:

Masterstudium Physik

Betreut von:

Univ.-Prof. Dipl.-Phys. Dr. Jannik C. Meyer

Abstract

In this thesis the atomic structure of ultrathin amorphous carbon films is studied. The films are created by evaporating carbon onto a salt crystal under vacuum. They are then transferred to a grid which provides free-standing areas of the film for microscopic analysis. The films are then observed in the TEM for a first analysis considering also the electron diffraction patterns. Afterwards, the films are investigated in the STEM which allows to record images with atomic resolution. These images are analysed by doing ring statistics which provide information about the amorphousness of the carbon films. The calculated crystallinity of the films results as $C = 0.597$. Additionally, AFM analysis is done to estimate the thickness of the carbon films and to compare the results to the information provided by the quartz thickness measurement system installed at the evaporator.

Zusammenfassung

In dieser Arbeit wird die atomare Struktur von ultradünnen amorphen Kohlenstofffilmen untersucht. Diese Filme werden hergestellt, indem Kohlenstoff im Vakuum auf einen Salzkristall aufgedampft wird. Darauf werden die Filme auf einen Probenhalter transferiert, der es ermöglicht freistehende Teile des Films im Mikroskop zu analysieren. Die Filme werden dann im TEM erstmals betrachtet, wobei auch die Beugungsbilder in die Analyse mit einfließen. Daraufhin werden die Filme im STEM untersucht, das Bilder mit atomarer Auflösung ermöglicht. Diese Bilder werden dann für eine Ringstatistik herangezogen, die Auskunft über die Amorphität der Probe gibt. Die daraus berechnete Kristallinität ergibt sich zu $C = 0.597$. Außerdem wird eine AFM-Analyse durchgeführt, um die Dicke der Kohlenstofffilme zu messen und mit den Werten zu vergleichen, die das Quartz-Dickenmesssystem liefert, das am Verdampfer installiert ist.

Acknowledgements

First I would like to thank my supervisor Prof. Dr. Jannik C. Meyer for the possibility to work in his group and for his great guidance throughout this thesis.

Furthermore, I want to express my gratitude to Dr. Franz Eder and to Dr. Jani Kotakoski for accompanying me during all the experiments and for taking always the time to deal with my questions. I also want to thank Mag. Dr. Clemens Mangler who introduced me to the STEM and helped me with all my problems regarding the microscope.

Of course I would also like to thank all members of the Nanostructured Materials group for providing such a pleasant and helpful environment.

Very special thanks go to my girlfriend Michaela for her encouragement, her support, and her patience in the last years.

Last but not least, I would like to thank my parents for making my studies possible and for supporting me in everything I do.

Contents

1	Introduction	1
2	Experimental Methods	3
2.1	Electron Microscopy	3
2.1.1	Transmission Electron Microscope	3
2.1.2	Scanning Transmission Electron Microscope	8
2.2	Atomic Force Microscopy	10
2.3	Sample Preparation	12
2.3.1	Evaporation onto Salt Crystals	12
2.3.2	Transfer to TEM-grids	13
3	Results and Discussion	15
3.1	TEM Measurements	15
3.1.1	Diffraction Analysis	18
3.2	AFM Measurements	20
3.3	STEM Measurements	22
3.3.1	Ring Statistics	25

4 Summary and Outlook	31
A Images for Ring Statistics	33
List of Figures	42
Bibliography	45

Chapter 1

Introduction

Since over 200 years, amorphous materials have been studied by researchers in the whole world. In 1932, Zachariasen described the structure of glass as a random atomic network such that there is no crystalline character in the atomic arrangement of amorphous materials [1]. Contrary theories claim that glass consists of a set of small crystals or of a composition of ordered and less ordered regions [2].

However, it was not possible to directly image the atomic structure of disordered structures until quite recently. Therefore, just a few studies regarding the atomic structure of amorphous materials have been done up to now, namely on two-dimensional silica glass [3, 4] and on amorphized graphene [5, 6].

In this thesis, the atomic structure of ultrathin amorphous carbon films will be investigated. Already in 1979, Isaacson et. al. studied the structure of thin amorphous carbon films using scanning transmission electron microscopy [7, 8]. To create the films, they simply evaporated carbon onto salt crystals. Since it was not possible yet to atomically resolve the carbon structures at that time, they indeed derived some results regarding the structure of the films, but not at an atomic level.

Due to the recent developments in atomic resolution electron microscopy, we are now able to study such two-dimensional amorphous carbon films regarding their atomic structure. For this purpose, carbon films are created by carbon evaporation onto salt, based on the work of Isaacson [7, 8] to get similar amorphous films. These films are then observed in the transmission electron microscope and in the atomic force microscope for a first analysis regarding their structure on a micrometer scale and their thickness variations. Finally, they are investigated in the atomic resolution

scanning transmission electron microscope to study their structure on a nanometer scale and to analyse their two-dimensional atomic structure.

But first of all, the experimental methods used during the experiments for this thesis should be briefly introduced in the following chapter.

Chapter 2

Experimental Methods

2.1 Electron Microscopy

Electron Microscopy is a very powerful and widely used method for imaging the surface or the inner structure of many different kinds of samples. For imaging the surface of a sample, the scanning electron microscope (SEM) is used where a point-shaped electron beam is scanning the sample, backscattered or secondary electrons are detected and, thus, contrast information of every scanned point of the probe is gathered. To investigate the inner structure of a sample, the transmission electron microscope (TEM) is suitable. Here, the electron beam is transmitted through a very thin sample and the projection of the irradiated area is mapped onto a screen. A combination of SEM and TEM leads to the Scanning Transmission Electron Microscope (STEM) where the electron beam is scanning the sample, but the transmitted electrons are detected.

Since TEM and STEM are the two types of electron microscopes which have been used frequently in the experiments for this thesis, they will be treated more in detail in the following sections.

2.1.1 Transmission Electron Microscope

More than 80 years have passed since Ernst Ruska and Max Knoll constructed the first transmission electron microscope in 1931 [9]. According to De Broglie, the

wavelength λ of an electron is decreasing with increasing momentum p :

$$\lambda = \frac{h}{p}$$

Hence, electrons are accelerated with acceleration voltages up to 3 MV [10] to reach very small wavelengths. For instance, an electron accelerated with 300 kV has a wavelength of approximately 2 pm. This enables the construction of microscopes with very high resolution. However, the most limiting factor for the resolution of electron microscopes is the lens aberration of the magnetic lenses. Therefore, aberration correctors consisting primarily of quadrupole, hexapole and octupole lenses have been developed in the last years. Since aberration correction is a very complex topic, a detailed treatment would go beyond the scope of this thesis. An extensive explanation of the topic can, for instance, be found in chapter 3 of reference [11]. Modern aberration corrected microscopes reach resolutions in the scale of Ångström are able to record atomically resolved images [12].

The schematic layout of a typical TEM is shown in Fig. 2.1. The electron gun is located on the top of the microscope followed by the system of condenser lenses. Inside the electron gun the electrons are emitted to the vacuum by thermionic emission using tungsten filaments or lanthanum hexaboride crystals, by field emission, or by hybrid forms. Then, the electrons are accelerated to the requested energy and focused on the sample by the condenser lenses. For illuminating the selected area of the sample homogeneously, it is important that the condenser system provides a parallel electron beam, as indicated in Fig. 2.1. Below the condenser system, the sample is placed. The electrons transmitted through the sample are then collected by the objective lenses and a system of intermediate lens and projector lens projects the magnified image onto a fluorescent screen or a CCD detector. Since the electrons have to pass through the sample, it is necessary that the sample is thin enough. The maximal thickness of the sample lies, depending on the acceleration voltage and on the atomic number of the samples material, in the range of a few hundred nanometers.

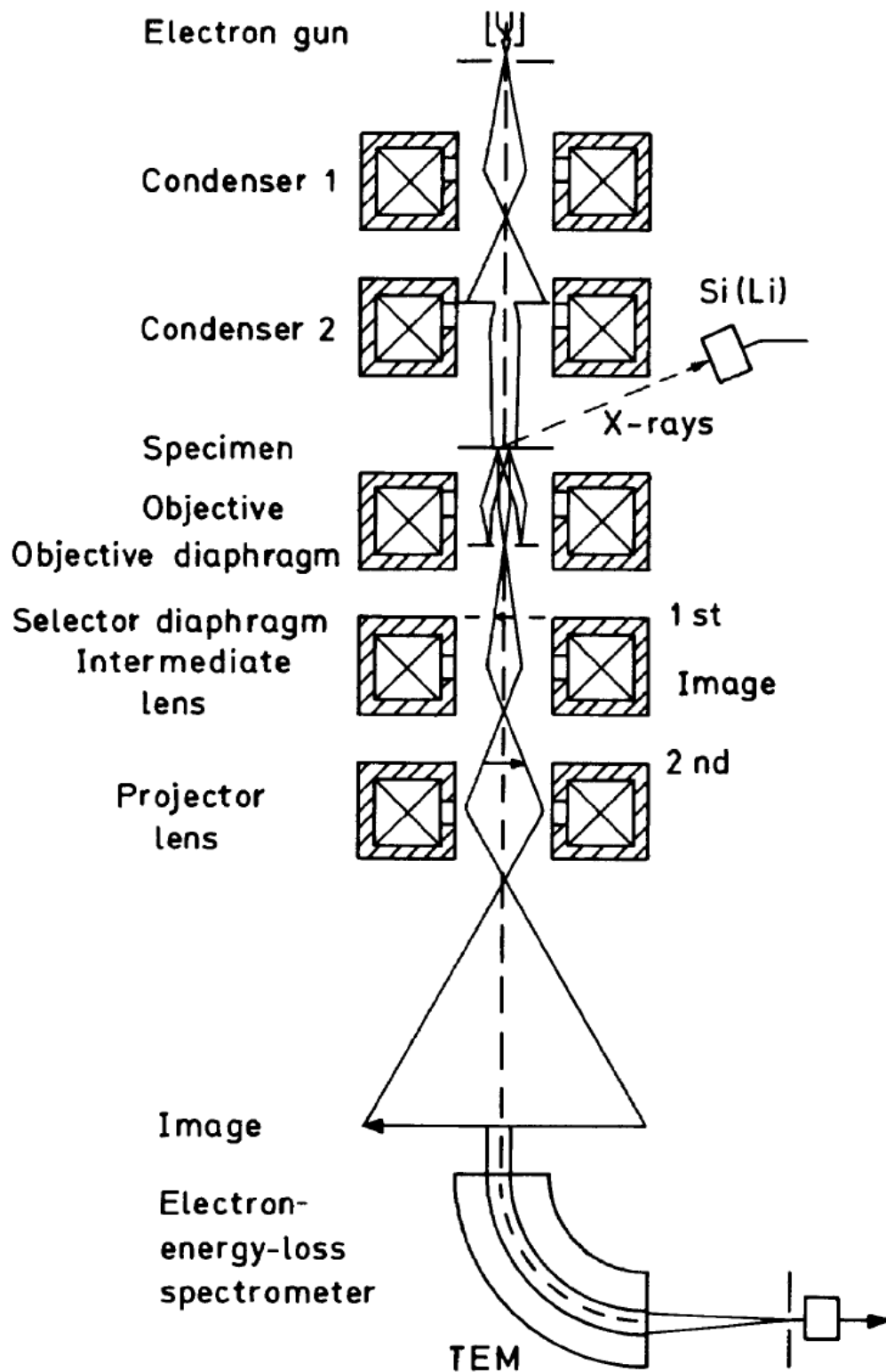


Figure 2.1: Schematic layout of a TEM with extensions for energy dispersive X-ray spectroscopy and electron energy loss spectroscopy (taken from reference [10])

Due to the fact that the interaction of the electron beam with the sample is not just given by elastic scattering, modern TEMs mostly have different extensions, which allow to analyse the sample besides imaging. For example (see Fig. 2.1), chemical analysis can be done using X-ray detectors to detect the characteristic X-rays of the sample for doing energy dispersive X-ray spectroscopy (EDX), and also inelastically scattered electrons contain information about the chemical composition of the sample and can be analysed using electron energy loss spectroscopy (EELS).

A special and very useful feature of the TEM is its ability to make the diffraction pattern visible, which is formed in the back focal plane of the objective lens. In this so called diffraction mode, the intermediate lens is set such that its object plane corresponds to the back focal plane of the objective lens. Thus, the diffraction pattern is projected onto the screen. Fig. 2.2 illustrates the ray path of the electron beam for both the imaging mode and the diffraction mode. In the imaging mode, all electrons that permeate the sample at a certain point are focused to one point also on the screen. In contrast, using the diffraction mode all electrons which are scattered in the same angle form one single spot on the screen. In many cases, e.g. for investigating polycrystalline samples, it can be useful to select just small areas of the sample for a diffraction pattern. For this purpose, a selected area diffraction (SAD) aperture is usually installed (see Fig. 2.2). Another aperture in the back focal plane of the objective lens can be used to choose certain parts of the transmitted electron beam. For better contrast, the continuous, unscattered beam can be selected to form the image (bright field image), and e.g. for orientation analysis, scattered beams can be chosen (dark field image).

The TEM used in the experiments for this thesis is a LVEM5, which works with a Schottky ZrO/W thermal field emission electron source and an acceleration voltage of 5 kV [13].

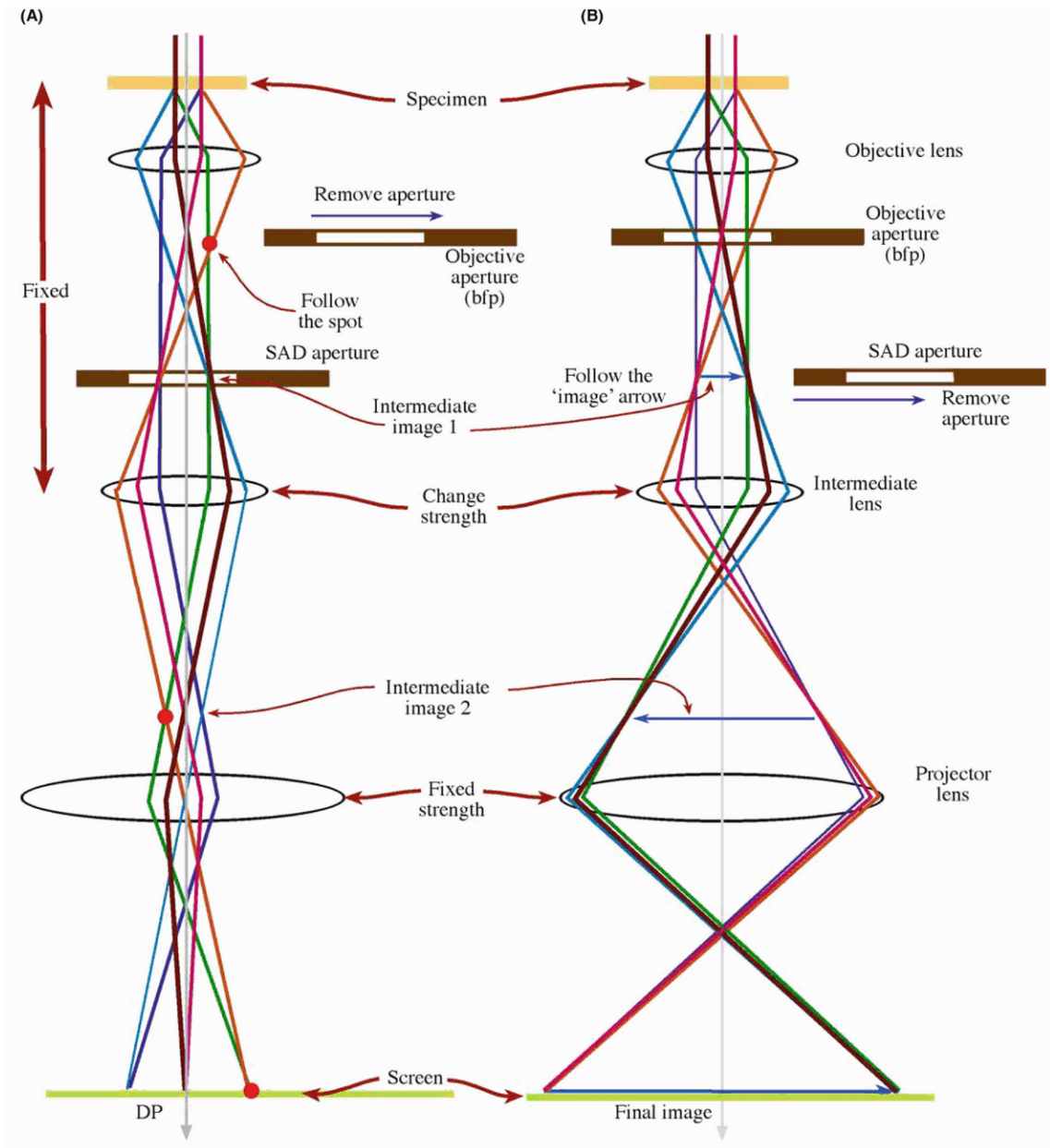


Figure 2.2: Ray path in a TEM between sample and screen of (A) the diffraction mode and (B) the imaging mode (taken from reference [14])

2.1.2 Scanning Transmission Electron Microscope

As already mentioned, in a STEM the image of a certain sample area is not formed by illuminating the selected area, as it is in a TEM, but by scanning the sample point by point with a very small-sized electron beam. This allows not just atomic resolution, but offers also many possibilities for material characterisation at the atomic level. The first STEM was build by Albert Crewe and his group in 1963 [15].

In principle, the setup of a STEM is similar to that of a TEM, but with the difference that the positions of electron gun and screen are switched (see Fig. 2.3). According to the reciprocity principle, which is based on the time reversal symmetry of ray diagrams, the bright field image of a STEM is equivalent to the bright field image of a TEM [10, 16]. The reason for this is that, for phase contrast imaging, only the scattering angle of the elastically scattered electrons is crucial. Since this angle is obviously not depending on the direction of the ray path, the optical result is the same.

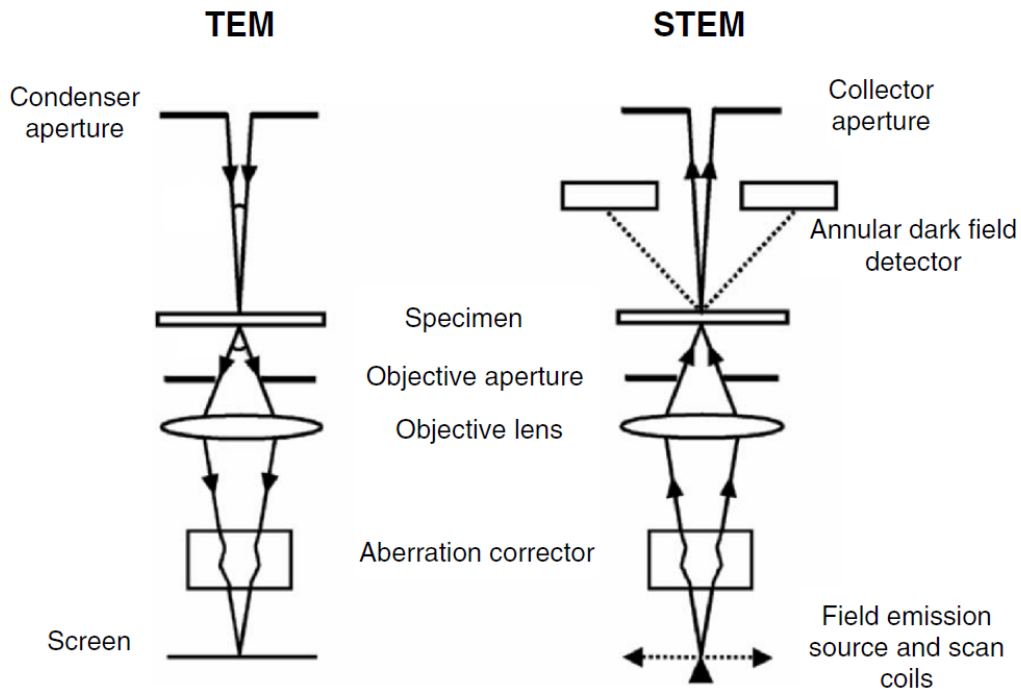


Figure 2.3: Illustration of the reciprocity principle in TEM and STEM (adapted from reference [16])

A major difference between TEM and STEM is the fact that the sample in a STEM is not hit by a parallel electron beam, but by a convergent electron probe, which is scanned across the sample. The primary aim is to get the smallest possible electron probe on the sample for obtaining the best resolution. Since lens aberrations are the main limiting factor for the probe size, aberration correction systems have been developed in the last years to improve the STEMs resolution. So, aberration corrected STEMs can reach resolutions up to 1 Ångström [17, 16].

The schematic layout of a modern STEM containing the main components is shown in Fig. 2.4 a. The electrons accelerated by the gun are first focused by the condenser lenses, before the aberrations are corrected in the aberration corrector. Then, the probe is passing the scan coils, which are responsible for moving the probe to scan across the sample. Before the transmitted electrons reach the detectors, they are passing a post sample lens system to maximize the efficiency at the detectors [5]. The detectors in the STEM are designed such that it is possible to simultaneously collect many signals. The bright field detector in the center detects the unscattered transmitted electron beam. Hence, holes in the sample appear bright in the image. In contrast, the annular dark field (ADF) detectors, which surround the direct beam, collect the scattered electrons and therefore holes appear dark in the images. The medium-angle ADF (MAADF) detector is used for small scattering angles, whereas the high-angle ADF (HAADF) detector collects the electrons scattered in a higher angle. Since the scattering angle increases with increasing atomic number Z of the samples material, the HAADF detector is also called Z -contrast detector [16].

Further analysis can be done with the EELS detector, where all other detectors are removed and the energy or rather the energy loss of the transmitted electrons is measured.

The STEM used for the experiments in this thesis is an UltraSTEM by Nion, depicted in Fig. 2.4 b [18, 19]. All STEM images in this thesis are recorded using the MAADF detector and an acceleration voltage of 60 kV.

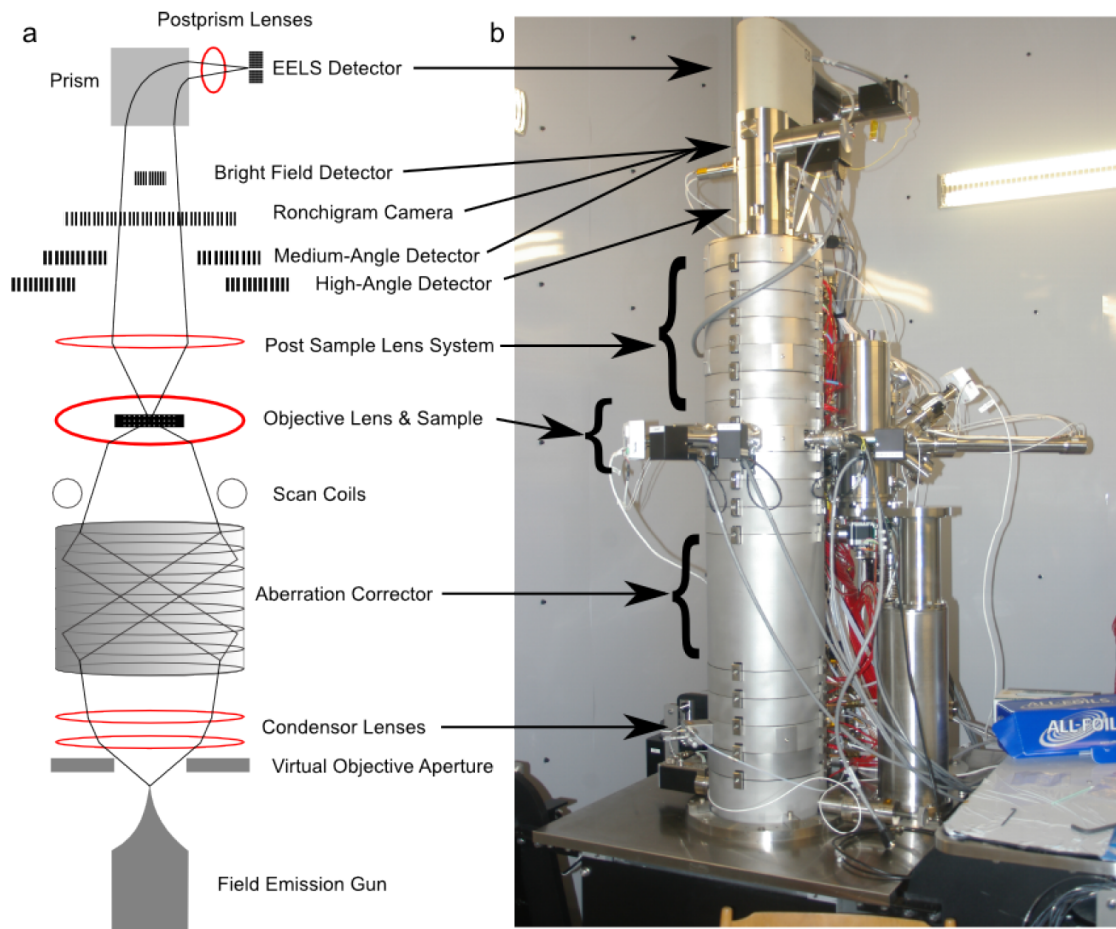


Figure 2.4: (a) Layout of a STEM containing the main components; (b) Photograph of the Nion STEM in Vienna used for the experiments in this thesis (taken from reference [5])

2.2 Atomic Force Microscopy

A further option to investigate the topography of a sample on an atomic scale is the atomic force microscope (AFM), invented by Binnig et al. in 1986 [20]. It is a very sensitive method, that allows imaging of a sample's surface with high resolution measuring the atomic forces between the sample and the AFM tip. The simplified schematic layout of an AFM is shown in Fig. 2.5. A cantilever with a very sharp tip is moved across the sample by the piezo actuator to scan the surface of the sample (both contact and non-contact modes are possible). A laser beam is focused onto the cantilever, which reflects the beam. The beam is then led to the

a quadrant photodiode that measures the deflection of the beam. Using this data, the topography of the sample can be reconstructed.

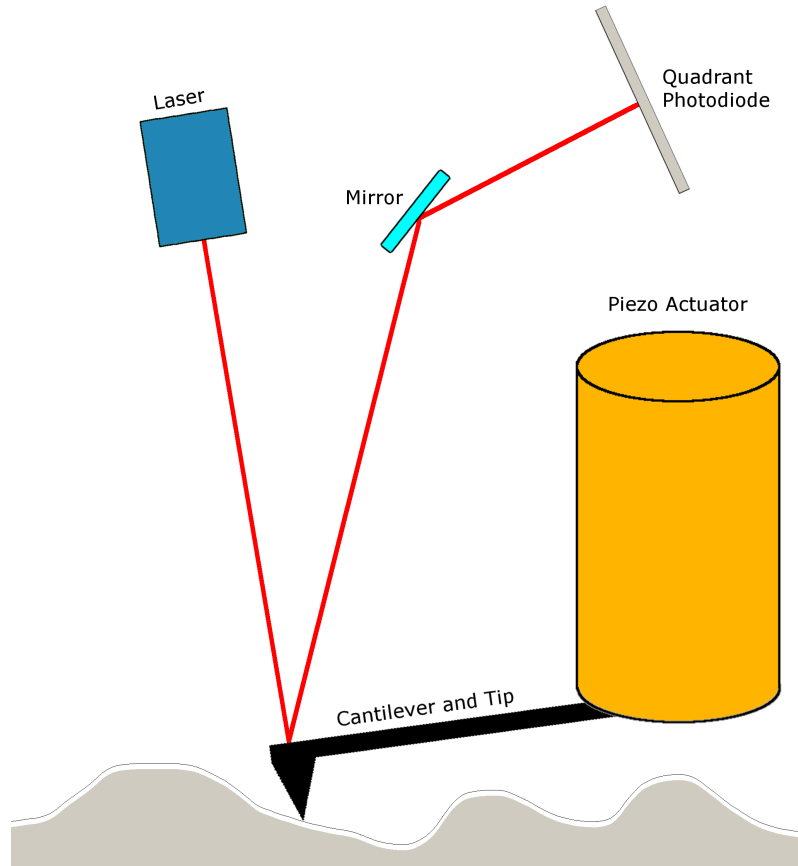


Figure 2.5: Schematic diagram of an AFM

The forces between the sample and the tip which are relevant for the AFM are primarily of electromagnetic nature. Depending on the distances, van-der-Waals interaction and repulsive interactions are the determining forces [21]. The big advantage of the AFM over other surface scanning techniques is its ability to investigate both conducting and insulating materials. Thus, a large variety of surfaces can be observed.

The microscope used for the experiments in this thesis is a Park Systems XE 100 AFM operating in a non-contact mode [22].

2.3 Sample Preparation

As already mentioned in chapter 1 the sample preparation, based on the work of Isaacson [7, 8], is done by evaporating carbon films onto monocrystalline salt. Then, the carbon films are transferred to special TEM grids, which allow to look at the samples in the electron microscopes. These two main steps in the sample preparation process will be described in more detail in the following sections.

2.3.1 Evaporation onto Salt Crystals

The reasons why the sodium chloride is used as substrate for the carbon films are both its very good solubility in water and its unwillingness to interact with carbon. To ensure that the area whereon the carbon is evaporated is well levelled, cultivated single salt crystals are used as substrates, so that the carbon films lie directly on the crystal planes of the salt. To get clean salt surfaces for each sample, little crystals are split in off from a bigger crystal by applying pressure with a sharp knife. In so doing, the wanted crystals break off in their crystallographic plane and provide perfectly even surfaces as substrates for the carbon films.

The evaporation of the carbon onto the salt is performed using a carbon wire and heating it up by electric current in vacuum. The salt crystal is placed below the carbon wire and so the carbon atoms evaporated from the wire arrange themselves randomly on the salt. The device used for this purpose was the Super Cool Sputter Coater EM SCD050 by Leica [23]. This instrument has installed a carbon thread evaporation mode which uses the flash evaporation method heating the thread up with a current of about 10 Ampere. The heating time can be controlled pushing a FLASH-Button for the desired evaporation time. The vacuum inside the evaporation chamber during the evaporation was in the range of $5 \cdot 10^{-2}$ mbar. For measuring the thickness of the evaporated film, the Leica EM QSG100 quartz film thickness monitor system was installed, which uses the relation between resonance frequency of the quartz and the mass of the evaporated material for thickness estimation.

The carbon films used for the following experiments are produced pushing the FLASH-Button for some tenths of a second. In this way, carbon films with measured thicknesses of about 1 nm could be achieved. In this thesis, all information regarding the thickness of the carbon films is given based on the just described thickness measurement system. How far this system gives accurate values for the

real thicknesses of the evaporated films, will be discussed in the further course of this thesis.

2.3.2 Transfer to TEM-grids

Once the carbon film lies on the salt, the next step is to transfer the film to special sample holders which allow to analyse the film in the electron microscope. In this case, the carbon films are transferred to a standard TEM-grids purchased from Quantifoil Micro Tools GmbH [24], which consist of gold bars forming a grid covered with a perforated carbon foil (see fig. 2.6). The whole grid is about 3 mm in diameter, the square holes in the gold grid have an edge length of about $100\ \mu\text{m}$, and the holes in the carbon foil are about $1.2\ \mu\text{m}$ in diameter. The thickness of the perforated foil is about 10 to 12 nm. The holes in the grid or rather in the covering foil provide free-standing parts of the sample such that influences on the measurements coming from the grid can be excluded.

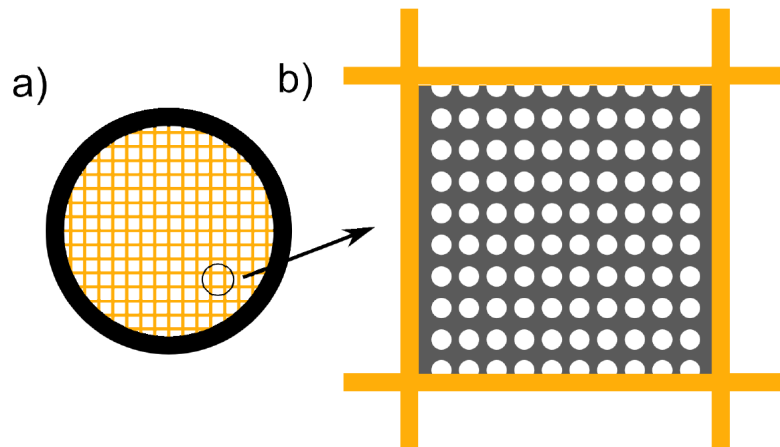


Figure 2.6: a) Illustration of the used TEM-grids consisting of gold bars; b) diagram of one magnified gold square of the grid to illustrate the perforated carbon foil (taken from reference [5])

To transfer the carbon film from the salt to the grid, the following steps are performed using some ideas from the transfer methods described in [25]. First, the TEM-grid is placed on the salt crystal such that the perforated carbon foil of the grid is in contact with the evaporated carbon film. To enhance this contact, a drop of Isopropanol is added that pulls the grid towards the film while it is evaporating.

For even better cohesion between film and grid, the sample is heated up to 200 °C for 10 minutes. Next, the salt crystal is slowly dissolved in water so that the grid covered with the evaporated film can be fished out. Subsequently, the grid is washed first again in water to remove any remaining salt residuals, and then in Isopropanol, which is reasonable to avoid damages because of its low surface tension compared to water. Once the Isopropanol is evaporated, the sample is ready for putting it into the TEM or the STEM.

Chapter 3

Results and Discussion

3.1 TEM Measurements

Since in the optical microscope it was not possible to see definitely whether the transfer from the salt to the TEM-grid was successful or not, one reason for looking at the samples in the TEM first was to figure out if the grids were well covered with the evaporated carbon film. Looking for little cracks in the film it was easy to find areas covered with carbon.

Besides that, some features in the carbon film have been found in the TEM images. Fig. 3.1 shows an image of a sample with a thickness of 1.4 nm. One hole of the perforated grid-foil is depicted where a crack in the film is visible and up to three layers of the carbon film on top of each other can be seen. According to QUANTIFOIL [24] the perforated carbon foil covering the gold grid is about 10 to 12 nm thick and obviously the three layers of the carbon film still appear brighter than the perforated foil, which appears black. Therefore, it is reasonable that the used thickness measurement system (see section 2.3.1) gives thickness values in the right order of magnitude. Since such multilayer areas have always been observed next to cracks in the film, they are probably caused by overlapping and are not grown like that during the evaporation process.

Another example for a feature in the carbon films appearing in the TEM is shown in fig. 3.2. Also here, one can see areas of the film with different thicknesses. However, in contrast to fig. 3.1 no crack is visible. The thicker part of the film seems to be rolled up at the edge and the thinner area is even thinner near the edge. Here, the

thicker area is probably not a double layer of the thinner area caused by overlapping but a feature due to the structure of the salt surface. Splitting the salt crystals in the crystallographic plane provides indeed large well-levelled areas but steps in the surfaces are unavoidable. It is very possible that in the evaporation process these steps cause differences in the thickness of the film and generate features such like in fig. 3.2.

Fig. 3.3 shows a TEM image of a sample where the transfer from the salt to the grid did not work as desired. The grid was almost completely uncovered and just a few little carbon flakes could be found on the grid. Additionally, these flakes look and behave different compared to the mostly continuous films of the well-transferred samples. On the one hand, the films look blotchy and very inhomogeneous in their thickness and, on the other hand, their shape changed under the electron beam and holes are formed, which never happened with the well-transferred samples. Since the evaporated film was quite thin (0.5 nm), it is conceivable that the film has been destroyed during the transfer process and that just randomly some carbon residuals remained on the grid forming little flakes. Further analysis of such samples (e.g. in the STEM) have not been done because it is almost impossible to retrieve these little flakes on an otherwise uncovered grid.

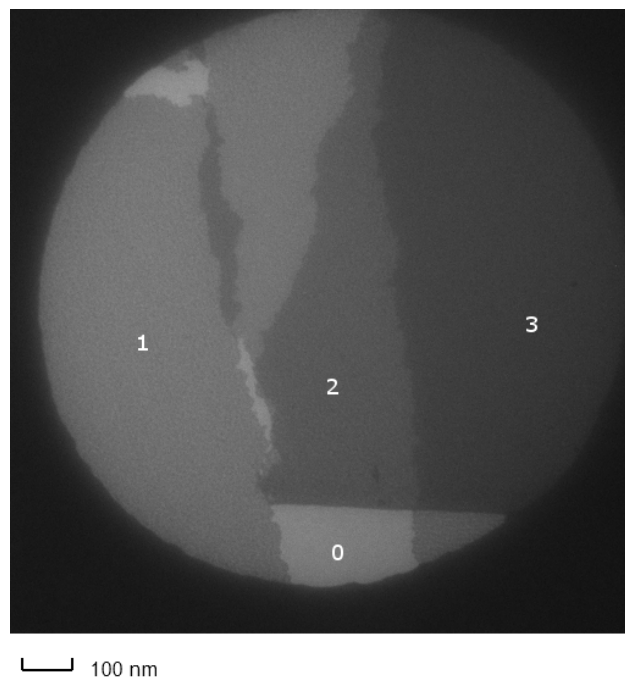
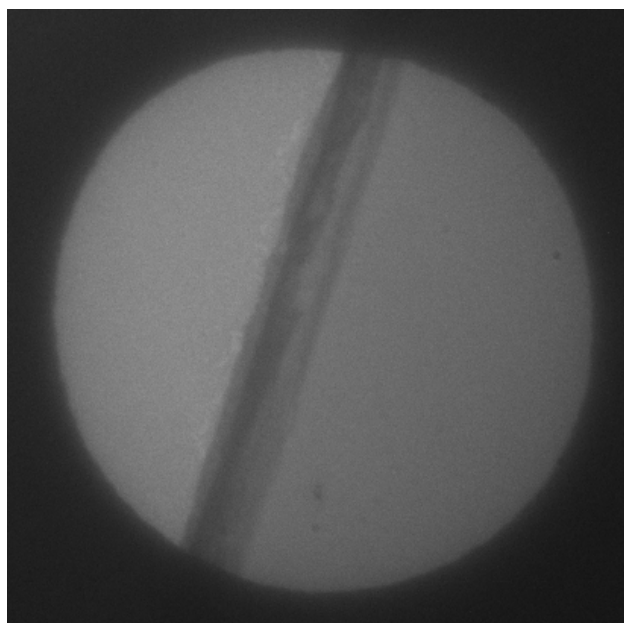
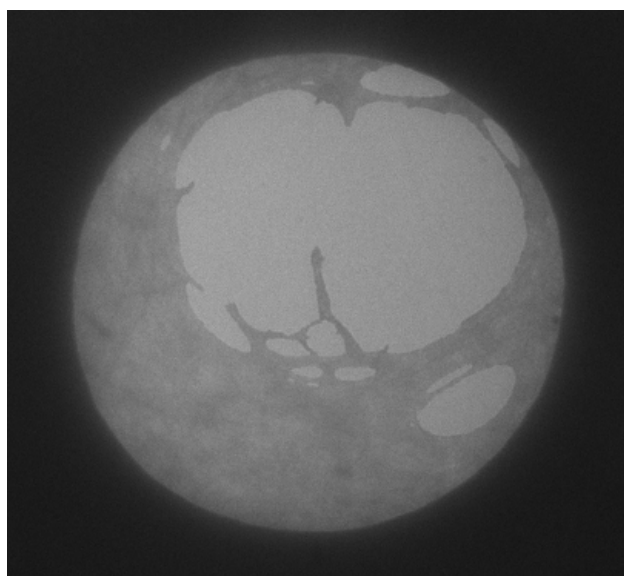


Figure 3.1: TEM image of a 1.4 nm thick sample showing a crack (0) and one (1), two (2), and three (3) layers of the carbon film.



└─┘ 100 nm

Figure 3.2: TEM image of an edge in a 2.2 nm thick carbon film probably caused by a step in the salt surface



└─┘ 200 nm

Figure 3.3: TEM image of an 0.5 nm thick carbon sample where the transfer was not successful, most of the grid was not covered with carbon, and just very few little carbon flakes could be found

3.1.1 Diffraction Analysis

For a first analysis of the atomic structure of the carbon films, the electron diffraction patterns are investigated using the TEM in the diffraction mode. The aim was to show that the evaporated films are of amorphous kind, which means that no crystalline character is appearing. Since the atomic structure in amorphous materials has no preferred direction, the electron diffraction pattern shows rings with radii referring to the bond lengths of the structure.

A diffraction pattern of a 1.5 nm thick film is shown in fig. 3.4, where the continuous beam and the rings of the first two diffraction orders can be seen.

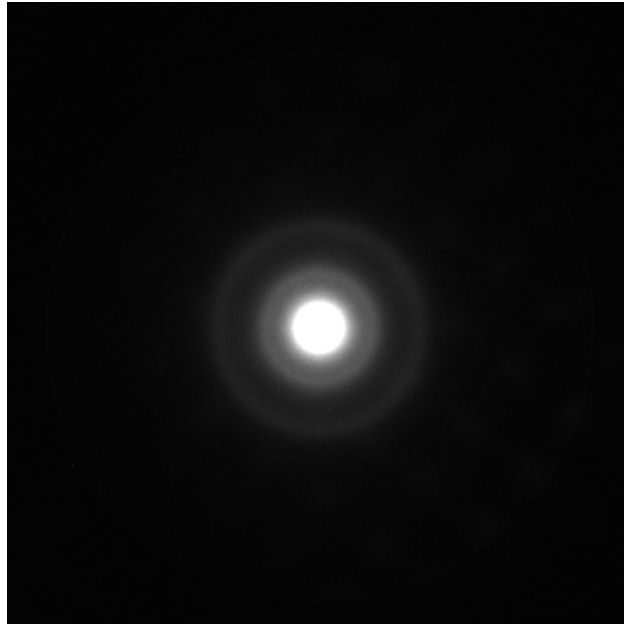


Figure 3.4: Electron diffraction pattern of a 1.5 nm thick amorphous carbon film

Very detailed studies about electron diffraction of amorphous carbon films have been done by Robertson and O'Reilly in [26] and [27], and by Kakinoki et al. in [28]. Among others, they investigated the films regarding the hybridisation of the carbon bonds, in other words, they proposed ratios of graphite-like (sp^2 -hybridized) and diamond-like (sp^3 -hybridized) carbon occurring in the film. While Robertson proposed the prevalent theory that 95% of the evaporated films is sp^2 -hybridized, Kakinokis approach revealed a 50% sp^2 - 50% sp^3 ratio. However, they both mention that the process of preparation is decisive for the structure of the films.

The carbon films produced for the experiments in this thesis are mostly of graphite-like structure. This can be seen in fig. 3.5 which shows an overlap of the diffraction pattern in fig. 3.4 with a diffraction pattern of pristine graphene. Obviously, the reflections in the graphene pattern lie on the rings of the amorphous film which indicates the same hybridisation.

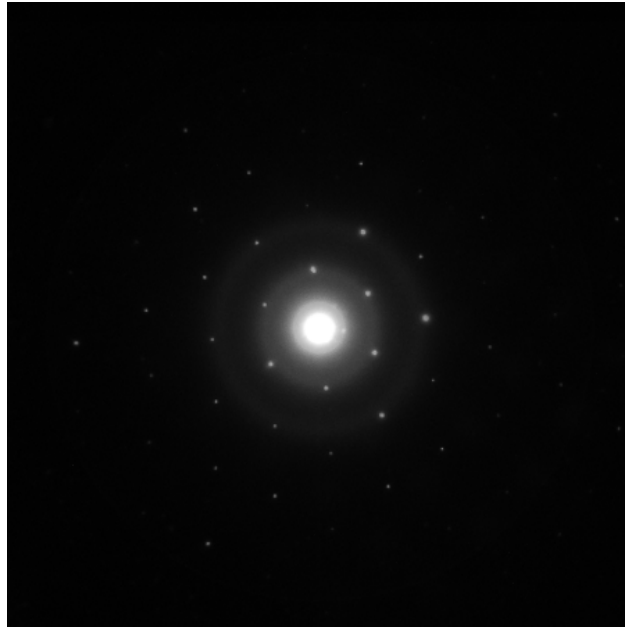


Figure 3.5: Overlay of the diffraction pattern in fig. 3.4 and a diffraction pattern of pristine graphene to show the sp^2 -structure of the carbon film

In total, 20 diffraction patterns of different areas on the amorphous film are recorded and no indication of diamond-like carbon could be found.

3.2 AFM Measurements

This section is concerned with the results of the AFM measurements on a carbon film with a nominal thickness of 0.8 nm according to the quartz balance. The main goal of the AFM analysis is to measure the thickness of the film in order to compare the results with the values provided by the quartz thickness measurement system. Since for good measurements a flat substrate is suitable, the carbon film is transferred onto a SiO₂ substrate using a method similar to the transfer method reported in [5]. First, a layer of Polymethylmethacrylate (PMMA) is spin coated onto the evaporated carbon film, and after baking it for 2 minutes at 160°C the salt is dissolved in deionized water. Then, the carbon film covered with PMMA is fished out of the water with the SiO₂ substrate, washed in isopropanol and water, and baked for 30 minutes at 160°C. Finally, the PMMA is dissolved by putting it into 1-Methyl-2-pyrrolidinone for 30 minutes at 120°C and then washed several times in acetone and isopropanol. Ideally, the carbon film lies on the SiO₂ substrate now.

The sample is now put into the AFM and the film is scanned using the AFM's non-contact mode. An AFM image of a sample area which contains holes, single layers and double layers of the carbon film is illustrated in fig. 3.6. In this image, profiles across the steps, i.e. between SiO₂ and first layer and between first and second layer, are investigated to determine the thickness of the film. An example for such a profile is shown in fig. 3.7 which is taken along the red arrow in fig. 3.6. In total, 58 profiles of steps are measured, and according to the profiles, the steps height between SiO₂ and the first carbon layer (49 profiles) is 4.1 ± 0.8 nm, and the steps height between first and second carbon layer (9 profiles) is 2 ± 0.6 nm. The difference in the step height can not be reasoned with certainty but one explanation might be that there is an adsorbed interlayer between the SiO₂ substrate and the first layer.

However, there is at least a factor 2 between the results of the AFM analysis and that ones provided by the quartz thickness measurement system. On the one hand, it has to be remembered that the measurement system installed at the evaporator gives a mean value regarding the whole film and that the AFM measurement is confined to a small sample area, but, on the other hand, the height difference relates to the fact that the quartz measurement system gives indeed thickness values in the right order of magnitude, but not with high accuracy.

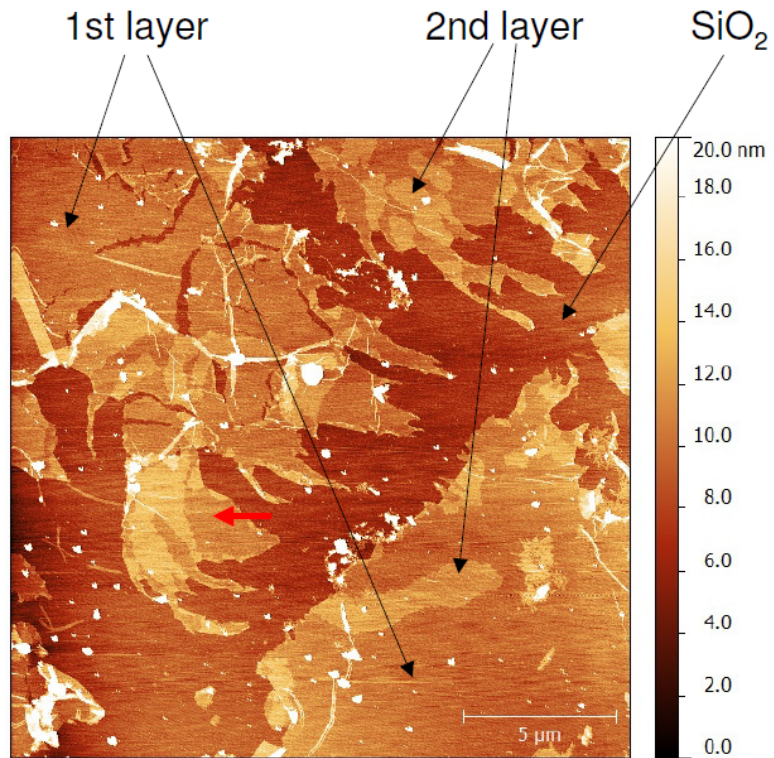


Figure 3.6: AFM image of an 0.8 nm thin carbon film showing single and double layers of the carbon film as well as holes in the film

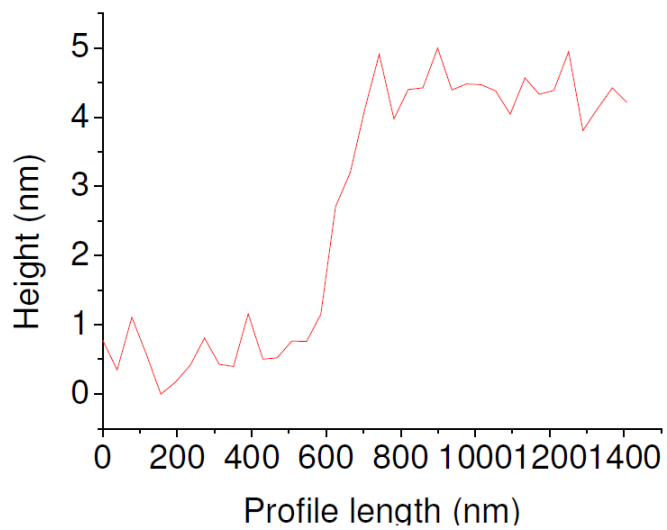


Figure 3.7: Height profile along the red arrow in fig. 3.6

3.3 STEM Measurements

For analysing the structure of the evaporated amorphous carbon films at the atomic level, the Nion UltraSTEM is a very powerful tool because of its ability to resolve atomic spaces. In this section, the results of the experiments at the STEM will be presented and an analysis concerning the films amorphousness at the atomic scale will be done.

The samples used for the STEM analyses are a nominally 1.4 nm thick and a nominally 0.8 nm thick carbon film. On both samples the grid was covered very well with the film and therefore it was not difficult to find covered area in the microscope. To resolve the atomic structure of the film it is necessary to find a two-dimensional area, i.e. an area where the film is consisting of just one layer of carbon atoms. An image of such a very thin area can be seen in fig. 3.8 showing an area of the 0.8 nm sample which contains a thicker part and a thinner part of the film. Obviously, the film is holey and porous in his thinner parts and it seems not very homogeneous, but as we will see later in this section there are some areas containing single atomic layers of carbon.

An image of how the thin parts of the 0.8 nm film looks observing an area of 32×32 nm is shown in fig. 3.10. Also here, the inhomogeneity of the film is evident and holes in the film can be seen as well as different numbers of carbon layers. At this scale, the images (fig. 3.8 – 3.10) look very similar to the images presented in the papers of Isaacson [7, 8] on which this thesis is based.

Due to the developments in high-resolution microscopy in the last years it is now possible to resolve structures which were not observable 30 years ago. Fig. 3.11 shows that Isaacson was not far away from seeing the structure of the two dimensional amorphous carbon. The image shows a field of 16×16 nm where areas of single atomic layers appear and the atomic structure of the film becomes visible. A further magnified image of a single atomic layer in the amorphous film can be seen in fig. 3.12 which shows the arrangement of the atoms in the two-dimensional amorphous film.

Since the film is very inhomogeneous in its thickness, the single-layer regions are not very large and it is not easy to find such areas. However, it has to be mentioned that the thinner film (0.8 nm) provides indeed more and larger single atomic layers than thicker one (1.4 nm), but single layers could be found in both films.

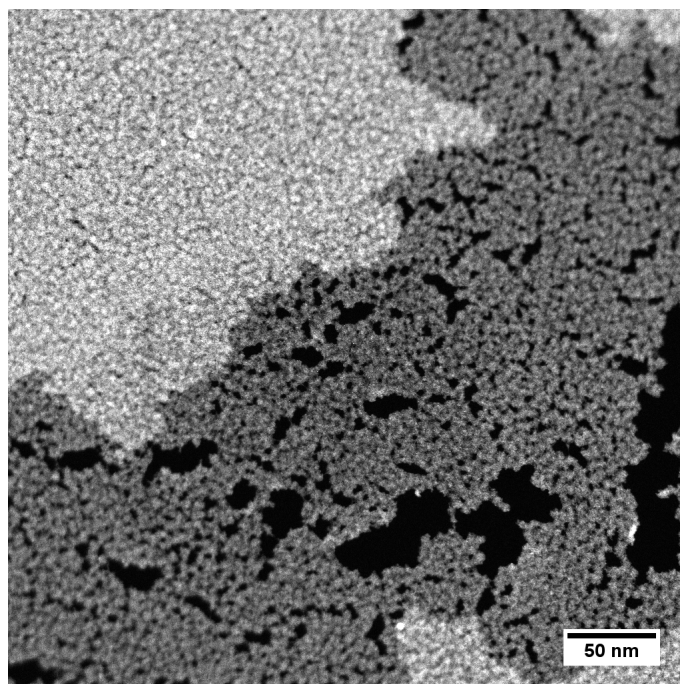


Figure 3.8: STEM image of an 0.8 nm thick carbon film showing an area of 384×384 nm with holes (black areas) and different thicknesses

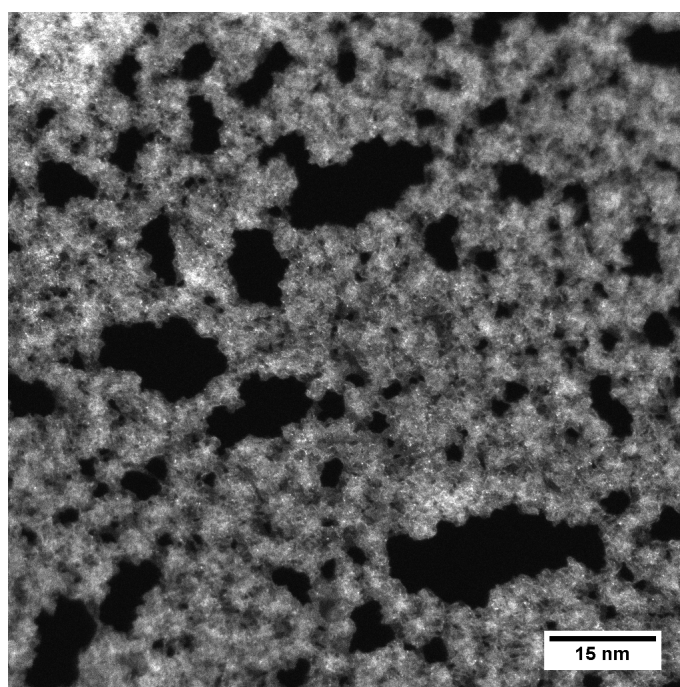


Figure 3.9: STEM image of an 0.8 nm thick carbon film showing an area of 96×96 nm with holes (black areas) and different thicknesses

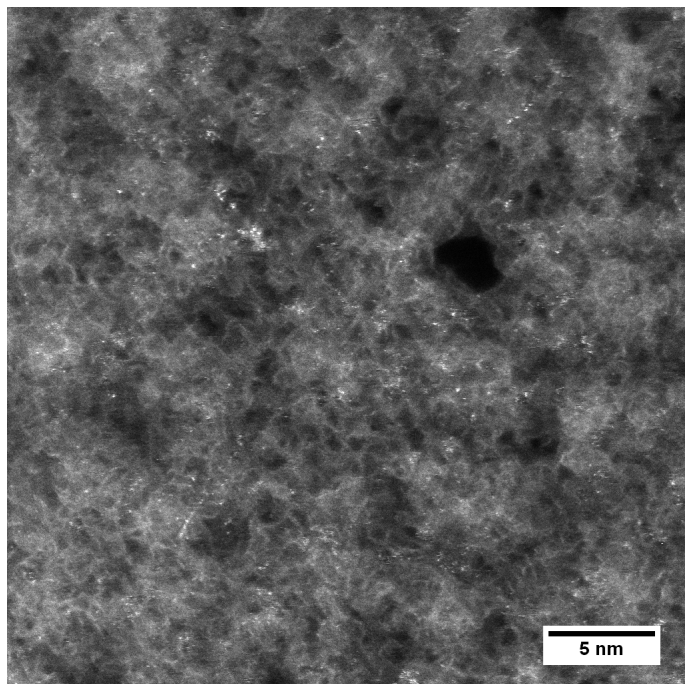


Figure 3.10: STEM image of an 0.8 nm thick carbon film showing the inhomogeneous structure similar to the images in [7, 8]; the black areas represent holes in the film

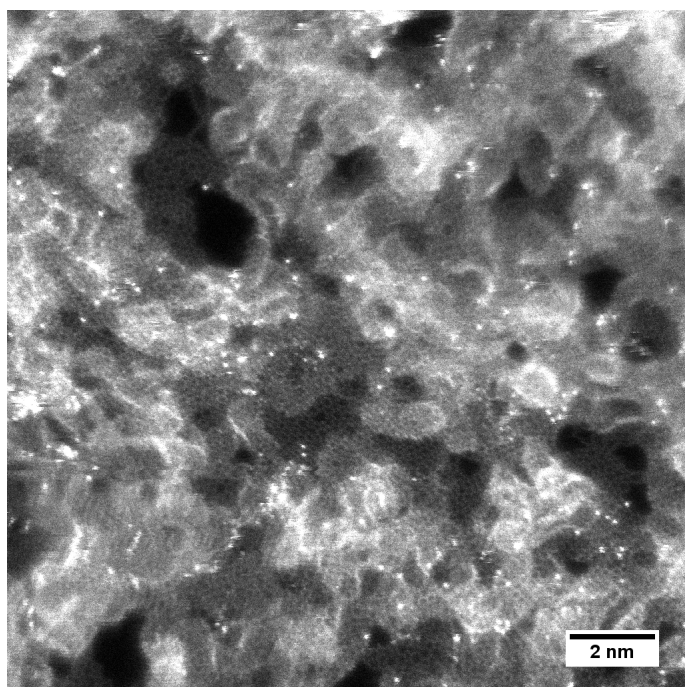


Figure 3.11: STEM image of an 0.8 nm thick carbon film showing areas where the atomic structure of the two-dimensional film is visible

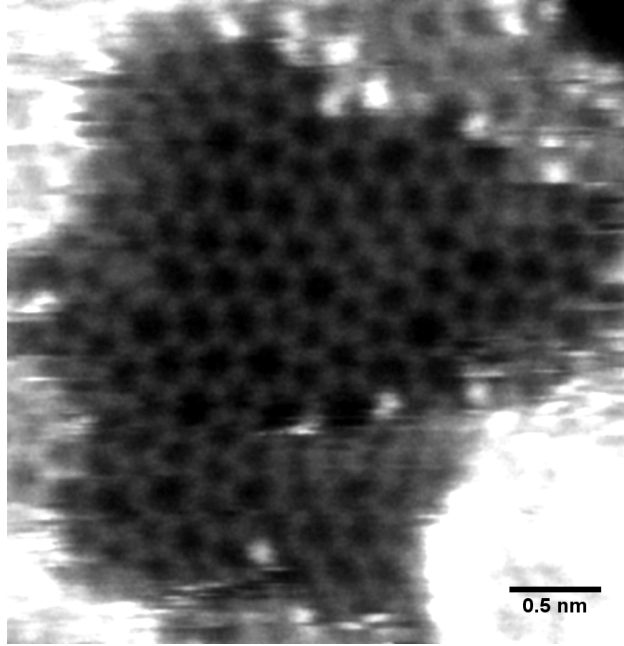


Figure 3.12: STEM image of an 0.8 nm thick carbon film showing the atomic structure of a single layer of the amorphous film

3.3.1 Ring Statistics

One way to analyse the amorphous two-dimensional carbon films is investigating their so called crystallinity C which is defined by the ratio of hexagons to all polygons in the film [4]. If the sample is perfectly crystalline, the crystallinity is equal to 1, and it decreases as the amorphousness of the sample is increasing. For example, pristine graphene has a crystallinity of $C = 1$, whereas a glassy silica film has a crystallinity of $C \approx 0.4$ [4, 3]. In this sense, C is also a measure for the amorphousness.

To calculate the crystallinity for the amorphous carbon films, it is necessary to analyse the images for knowing the number of hexagons compared to the number of all polygons. For this analysis, ring statistics have been done where all types of polygons appearing in the images are counted. For this purpose, carbon atoms are located in the images marking them with grey dots and these dots are then connected to get a model of the atomic structure. In this model, all different polygons can clearly be identified and counted. Fig. 3.13 shows this process based on the image shown in fig. 3.12. The figures 3.14–3.16 show some further examples for such analysis.

To get reliable results, a total of 38 images of both 0.8 and 1.4 nm thick films is analysed. The images which are used for the ring statistics in addition to the those shown in fig. 3.13–3.16 can be found in the appendix A.

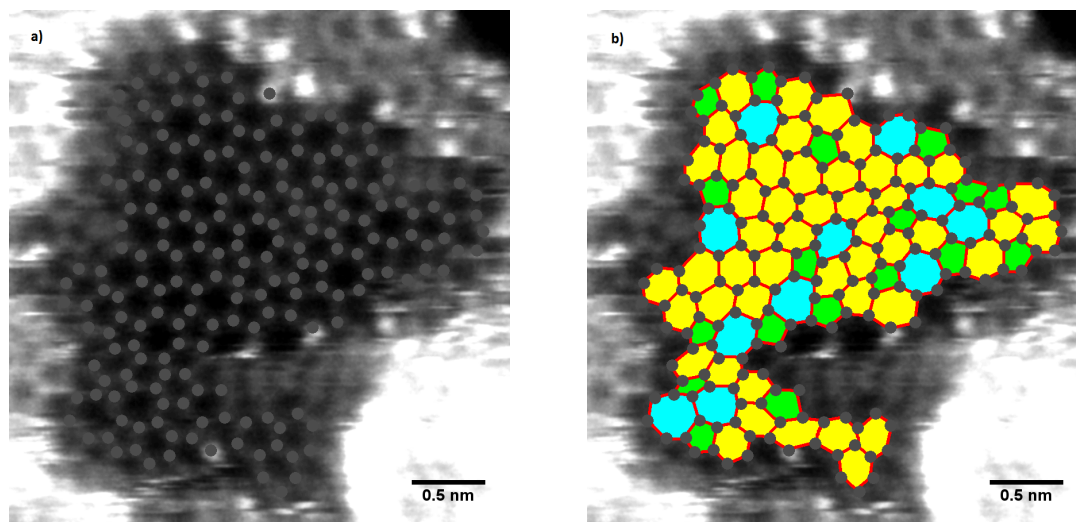


Figure 3.13: Steps in the process of image analysis for the ring statistics based on the image shown in fig. 3.12: a) atoms are marked with grey dots, b) polygons are identified in the model

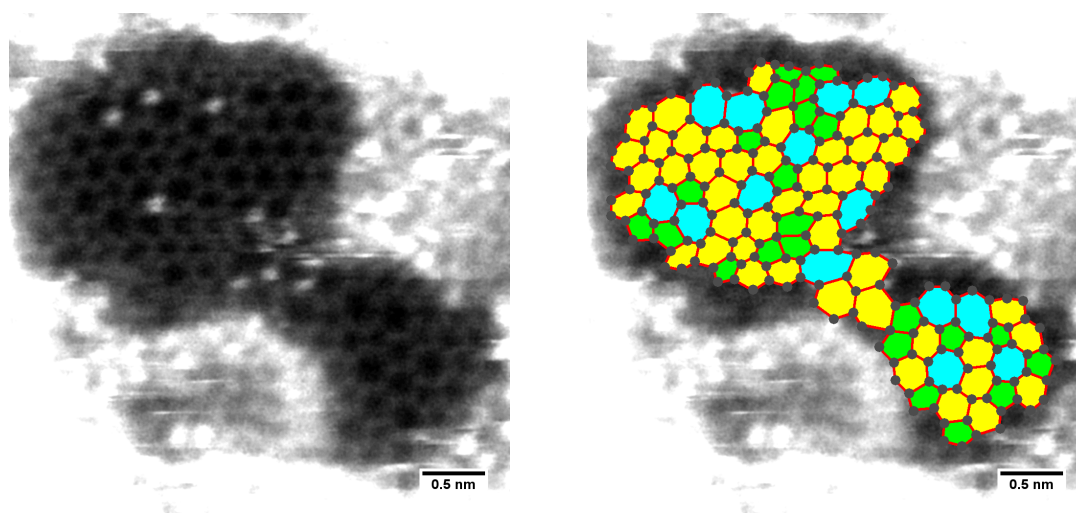


Figure 3.14: STEM image of an 1.4 nm thick carbon film (left) and corresponding ring analysis (right)

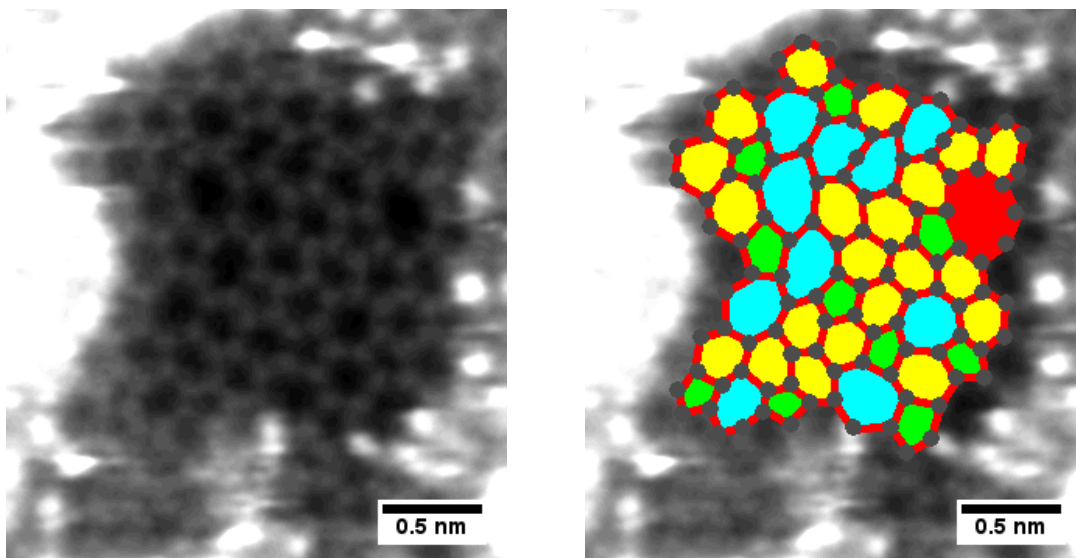


Figure 3.15: STEM image of an 1.4 nm thick carbon film (left) and corresponding ring analysis (right)

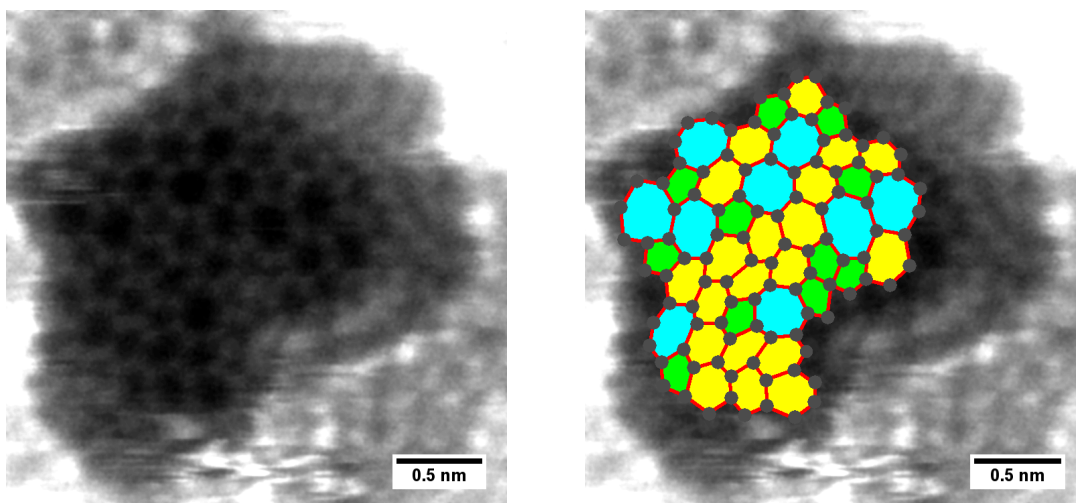


Figure 3.16: STEM image of an 1.4 nm thick carbon film (left) and corresponding ring analysis (right)

The ring statistics done on the mentioned 38 images yield the results shown in tab. 3.1, where both the number and the percentage of the different kinds of polygons is shown for all of the analysed images.

	tetragons		pentagons		hexagons		heptagons		octagons		nonagons	
	#	%	#	%	#	%	#	%	#	%	#	%
Fig. 3.13	0	0.00	18	23.38	48	62.34	11	14.29	0	0.00	0	0.00
Fig. 3.14	0	0.00	23	27.71	46	55.42	14	16.87	0	0.00	0	0.00
Fig. 3.15	0	0.00	10	23.81	21	50.00	10	23.81	1	2.38	0	0.00
Fig. 3.16	0	0.00	11	27.50	20	50.00	9	22.50	0	0.00	0	0.00
Fig. A.1	0	0.00	9	12.68	51	71.83	10	14.08	1	1.41	0	0.00
Fig. A.2	0	0.00	12	21.05	34	59.65	9	15.79	2	3.51	0	0.00
Fig. A.3	0	0.00	10	20.41	29	59.18	9	18.37	1	2.04	0	0.00
Fig. A.4	1	3.33	6	20.00	17	56.67	4	13.33	2	6.67	0	0.00
Fig. A.5	0	0.00	6	20.00	21	70.00	2	6.67	1	3.33	0	0.00
Fig. A.6	0	0.00	5	18.52	20	74.07	1	3.70	1	3.70	0	0.00
Fig. A.7	0	0.00	6	22.22	13	48.15	8	29.63	0	0.00	0	0.00
Fig. A.8	0	0.00	21	23.33	47	52.22	19	21.11	3	3.33	0	0.00
Fig. A.9	0	0.00	34	29.57	53	46.09	24	20.87	3	2.61	1	0.87
Fig. A.10	0	0.00	12	15.19	54	68.35	12	15.19	1	1.27	0	0.00
Fig. A.11	0	0.00	7	26.92	14	53.85	3	11.54	2	7.69	0	0.00
Fig. A.12	0	0.00	18	31.58	27	47.37	12	21.05	0	0.00	0	0.00
Fig. A.13	0	0.00	7	30.43	14	60.87	2	8.70	0	0.00	0	0.00
Fig. A.14	1	2.44	10	24.39	21	51.22	9	21.95	0	0.00	0	0.00
Fig. A.15	0	0.00	2	11.11	14	77.78	2	11.11	0	0.00	0	0.00
Fig. A.16	0	0.00	15	28.30	27	50.94	11	20.75	0	0.00	0	0.00
Fig. A.17	1	2.50	11	27.50	17	42.50	11	27.50	0	0.00	0	0.00
Fig. A.18	0	0.00	5	17.86	19	67.86	4	14.29	0	0.00	0	0.00
Fig. A.19	0	0.00	6	17.14	24	68.57	5	14.29	0	0.00	0	0.00
Fig. A.20	0	0.00	5	25.00	10	50.00	4	20.00	1	5.00	0	0.00
Fig. A.21	0	0.00	11	15.94	44	63.77	13	18.84	1	1.45	0	0.00
Fig. A.22	0	0.00	16	20.00	49	61.25	12	15.00	3	3.75	0	0.00
Fig. A.23	0	0.00	4	11.43	25	71.43	6	17.14	0	0.00	0	0.00
Fig. A.24	0	0.00	10	19.61	34	66.67	6	11.76	1	1.96	0	0.00
Fig. A.25	0	0.00	7	14.29	37	75.51	4	8.16	1	2.04	0	0.00
Fig. A.26	0	0.00	3	30.00	6	60.00	1	10.00	0	0.00	0	0.00
Fig. A.27	0	0.00	11	25.00	28	63.64	5	11.36	0	0.00	0	0.00
Fig. A.28	0	0.00	1	10.00	8	80.00	1	10.00	0	0.00	0	0.00
Fig. A.29	0	0.00	17	24.29	37	52.86	16	22.86	0	0.00	0	0.00
Fig. A.30	0	0.00	11	30.56	15	41.67	9	25.00	1	2.78	0	0.00
Fig. A.31	0	0.00	5	25.00	13	65.00	2	10.00	0	0.00	0	0.00
Fig. A.32	0	0.00	11	27.50	18	45.00	10	25.00	1	2.50	0	0.00
Fig. A.33	0	0.00	3	30.00	6	60.00	1	10.00	0	0.00	0	0.00
Fig. A.34	0	0.00	5	17.86	19	67.86	4	14.29	0	0.00	0	0.00

Table 3.1: Results of the ring statistics showing number and percentage of the appearing polygons for all of the images

The values collected in tab. 3.1 lead to the ring statistics shown in tab. 3.2 which presents the percentage of each kind of polygon in the images calculated by averaging.

tetragons:	$(0.22 \pm 0.12) \%$
pentagons:	$(22.29 \pm 0.97) \%$
hexagons:	$(59.73 \pm 1.64) \%$
heptagons:	$(16.23 \pm 0.98) \%$
octagons:	$(1.51 \pm 0.32) \%$
nonagons:	$(0.02 \pm 0.02) \%$

Table 3.2: Ring statistics showing the percentage of each kind of polygon appearing in the images

Since the percentage of hexagons corresponds to the crystallinity, C results to

$$C = (0.597 \pm 0.017)$$

It is claimed in [5] that, regarding carbon structures, the crystallinity is about $C = 0.5$ for completely disordered and amorphous structures. According to that, the evaporated carbon films can rightly be called amorphous.

For comparison, ring statistics have also been done on an amorphous carbon sample by Andrey Turchanin consisting of disordered membranes created via annealing of organic molecules on a metal substrate (similar to the samples in [29]). Two examples for atomically resolved images of Turchanins sample are shown in fig. 3.17. It can be seen that the crystalline areas of this sample are considerably larger compared to the amorphous evaporated carbon films. The ring analysis of Turchanins sample leads to a crystallinity of $C = (0.797 \pm 0.021)$ and therefore this sample could rather be called nanocrystalline than amorphous.

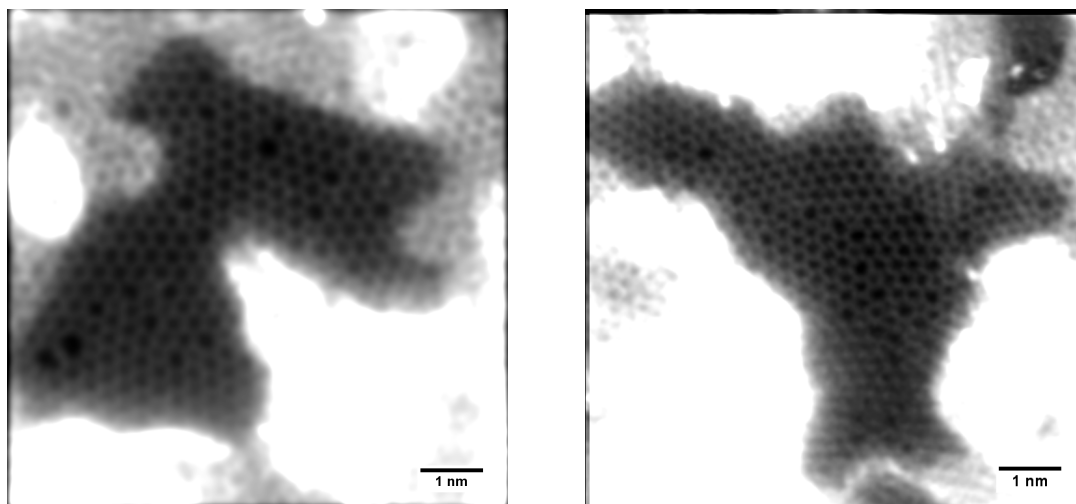


Figure 3.17: STEM images of a sample by Andrey Turchanin consisting of disordered membranes created via annealing of organic molecules

Chapter 4

Summary and Outlook

In this thesis the atomic structure of two-dimensional amorphous carbon films is investigated using different microscopic techniques. The films are created by evaporation of carbon onto a salt crystal which is in principle a very simple and cheap production method. The transfer to the TEM-grid works nicely and requires no polymer or similar assistance, which reduces the risk of destroying the sample during the transfer process.

For a first analysis, the films are observed in the TEM, on the one hand to check whether the grid is well covered with the carbon film and on the other hand to get a first impression of the structure of the film looking at different features like cracks, overlapping layers, and thickness variations. The electron diffraction patterns of the film are investigated using the TEMs diffraction mode. The diffraction patterns show the typical rings for amorphous structures which leads to the conclusion that the film is definitely not of a crystalline character. Additionally, a comparison of the diffraction patterns to the diffraction pattern of graphene suggests that the film is consisting of graphite-like structures.

The AFM analysis is done to measure the film thicknesses and to compare the results to the information provided by the quartz thickness measurement system installed at the evaporator. For this purpose, the film is transferred to a SiO₂ substrate to have flat surfaces for the AFM measurements. The results indicate that the values from the quartz measurement system are not reliable without restrictions, but they provide reasonable estimations.

Finally, two carbon films are observed in the STEM which allows to resolve the

atomic structure of the films. Since the film is rather inhomogeneous in its thickness at the atomic scale, the observed atomic single layer areas are not bigger than a few square nanometres, whereby the thinner film has larger single layer areas than the thicker one. However, atomically resolved images of the carbon films are recorded and then analysed by doing ring statistics. These analyses yield a crystallinity of $C = 0.58$ which implies high disorder and amorphousness.

Since this kind of amorphous carbon films is not very well researched, there are still many things to discover and, therefore, future experiments should focus on further characterisation. The formation of the films should be investigated, e.g. by doing simulations, to improve the evaporation process and to get larger areas of atomic single layers. The mechanical properties should be studied, for example by puncturing the film with the AFM tip and measuring force-distance curves. Also the electrical properties of the films could be interesting and should be examined, for instance doing transport measurements.

These are just a few ideas for further research on this very interesting two-dimensional structure.

Appendix A

Images for Ring Statistics

Here, the images used for the ring statistics in section 3.3.1 are shown. The images used for the ring statistics have been analysed like that one in section 3.3.1 using coloured markers to indicate the different polygons which are defined in the following way:

●	tetragon
●	pentagon
●	hexagon
●	heptagon
●	octagon
○	nonagon

In the following pages, all images can be found which have been used for the ring statistics. The scale bar is 0.5 nm in all images.

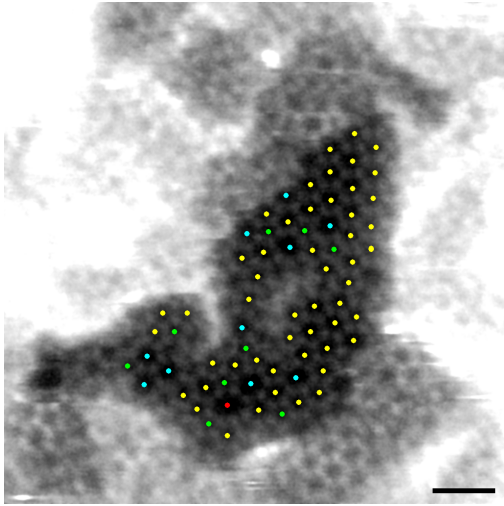


Figure A.1

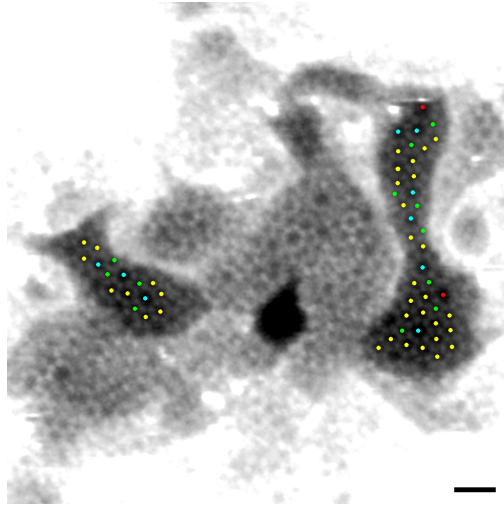


Figure A.2

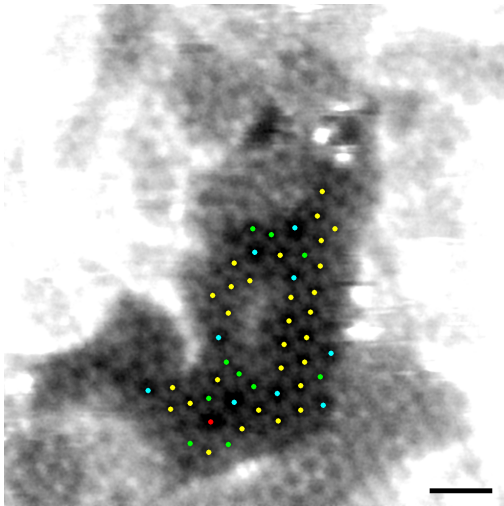


Figure A.3

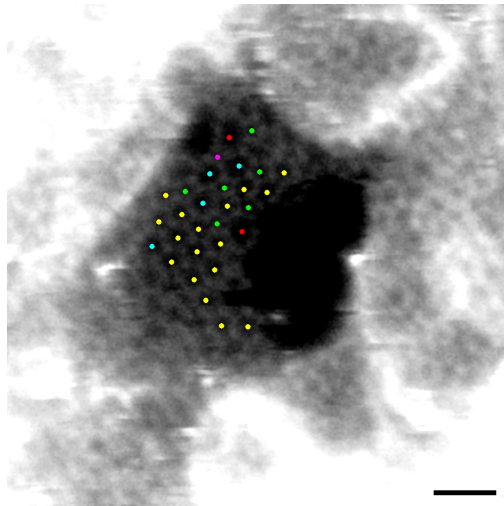


Figure A.4

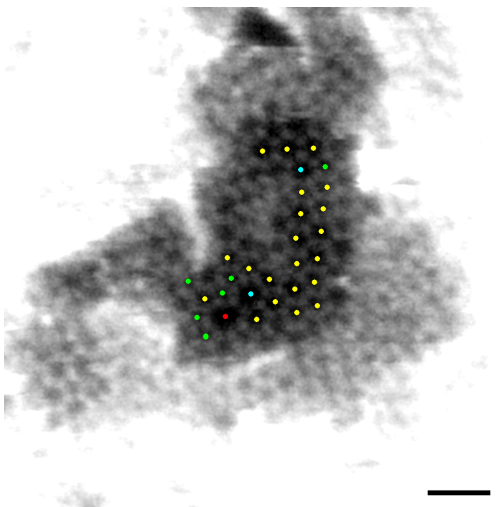


Figure A.5

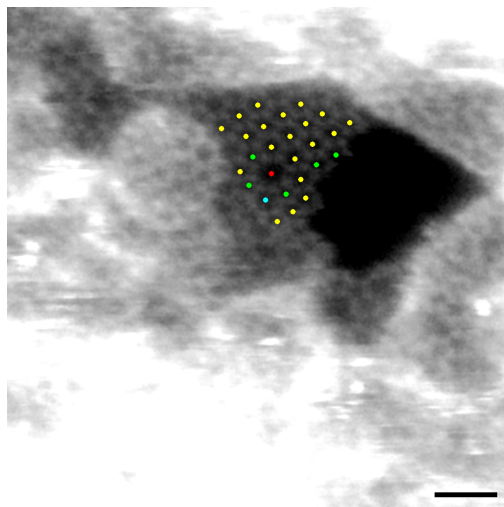


Figure A.6

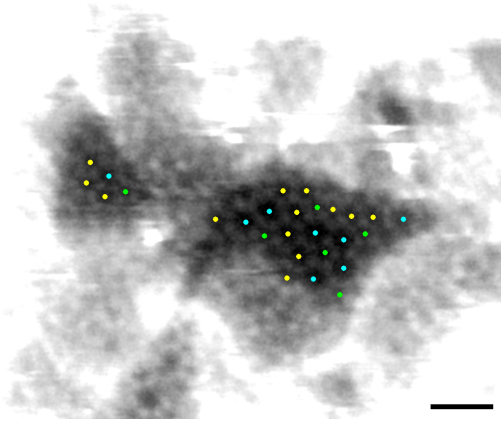


Figure A.7

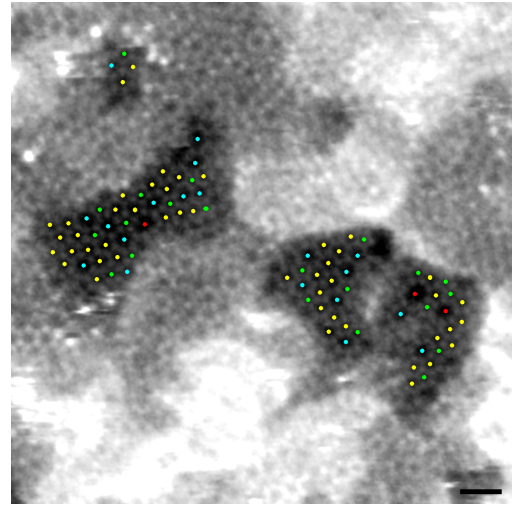


Figure A.8

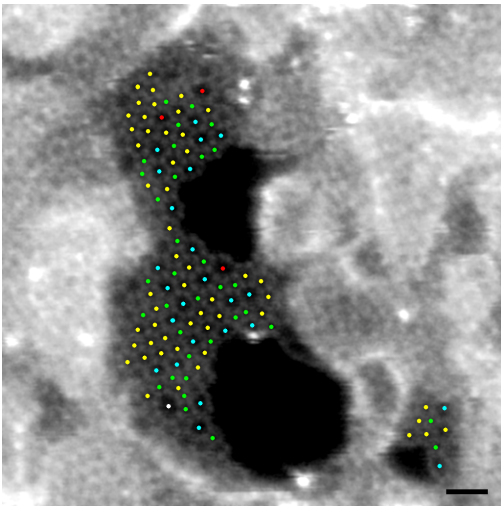


Figure A.9

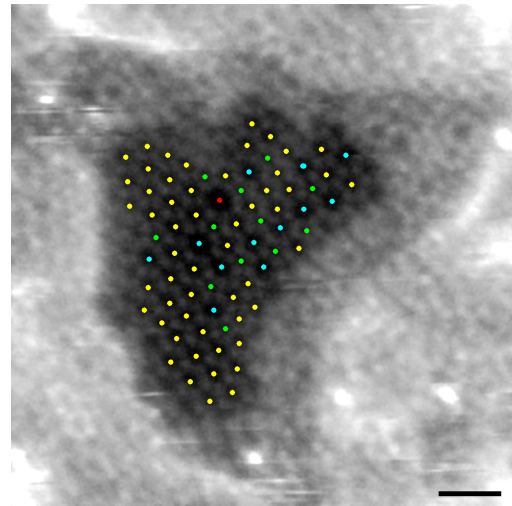


Figure A.10

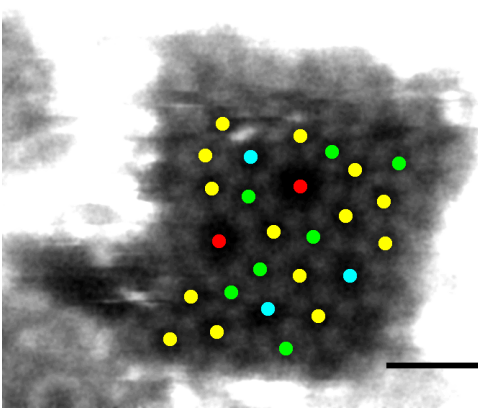


Figure A.11

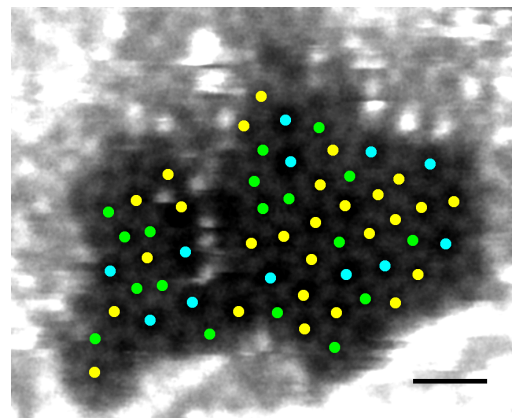


Figure A.12

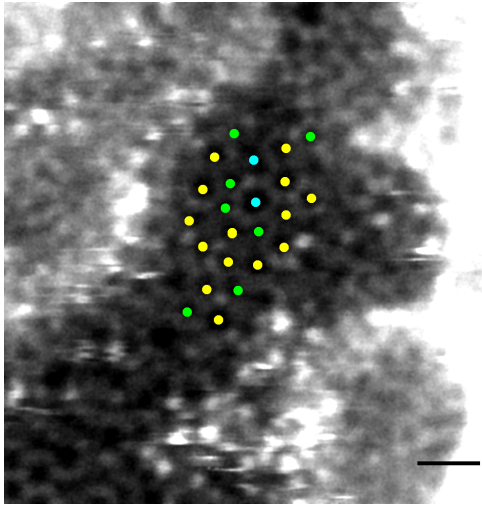


Figure A.13

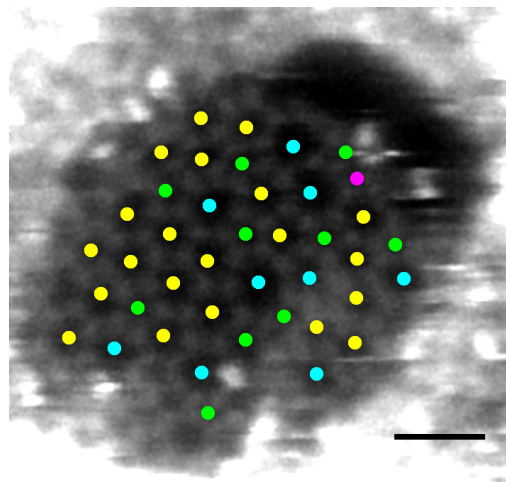


Figure A.14

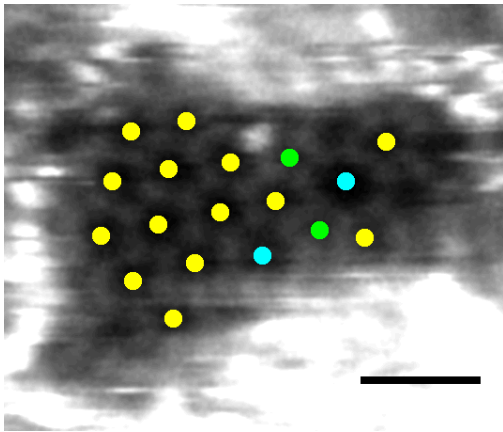


Figure A.15

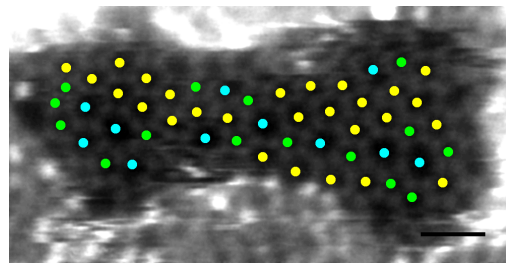


Figure A.16

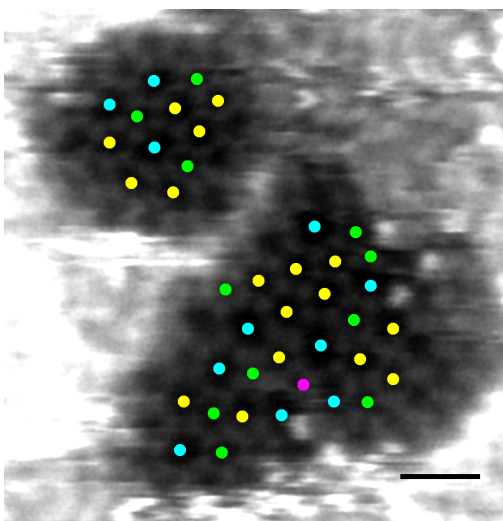


Figure A.17

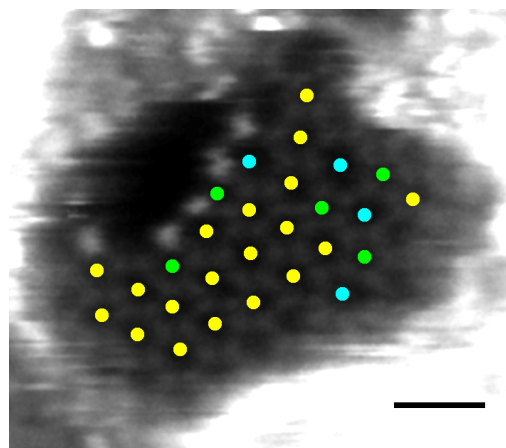


Figure A.18

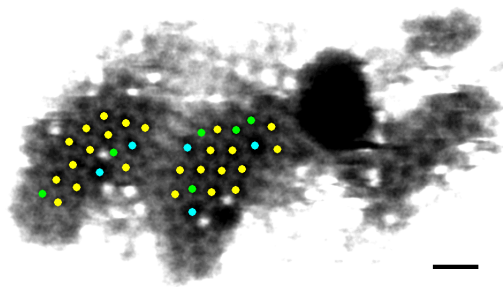


Figure A.19

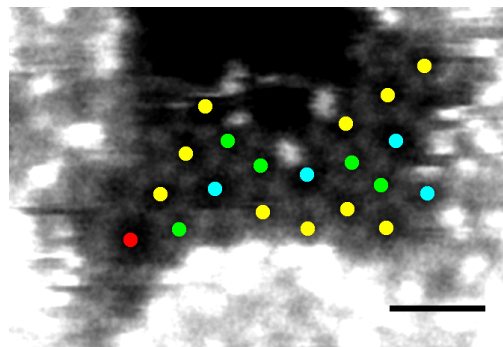


Figure A.20

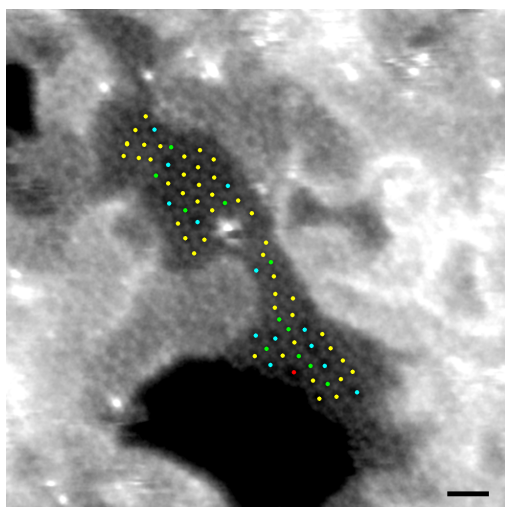


Figure A.21

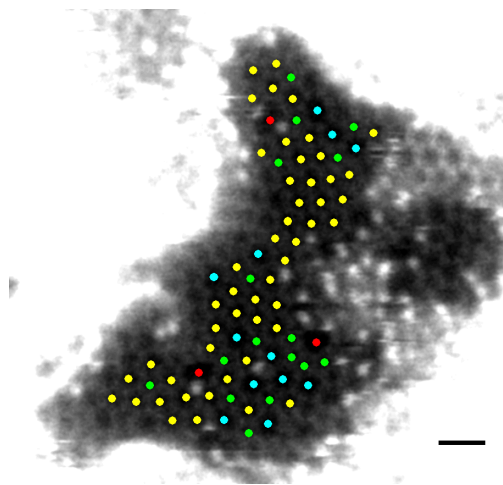


Figure A.22

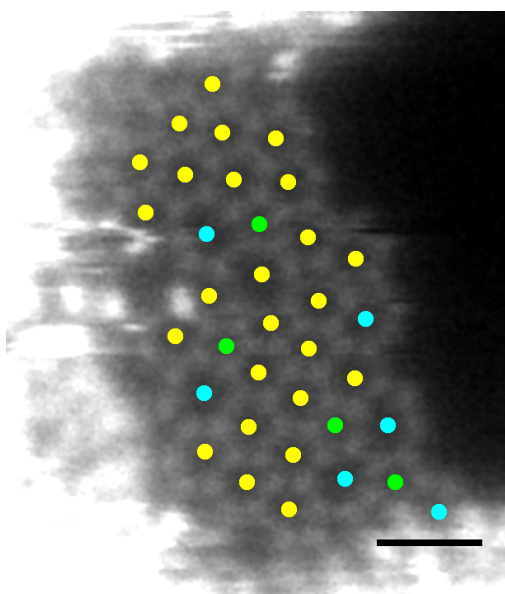


Figure A.23

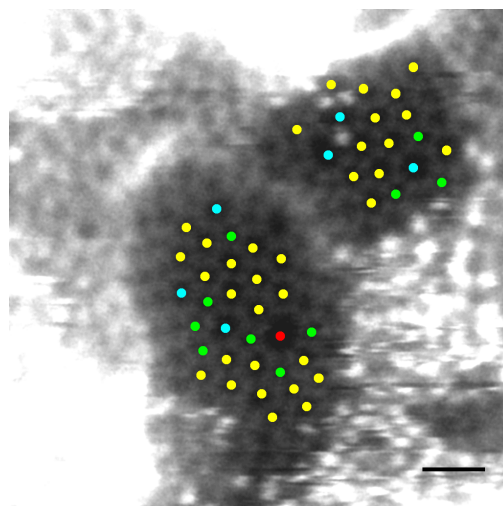


Figure A.24

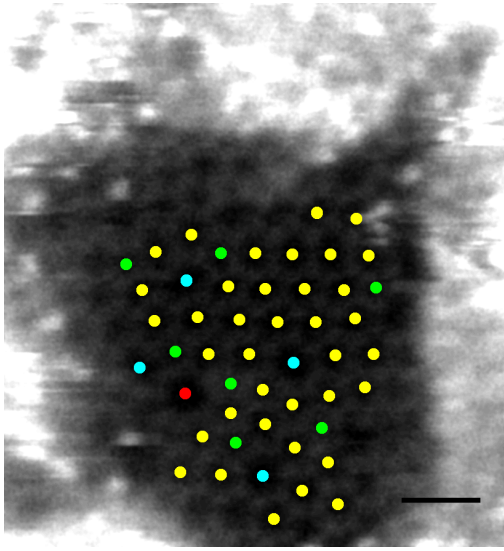


Figure A.25

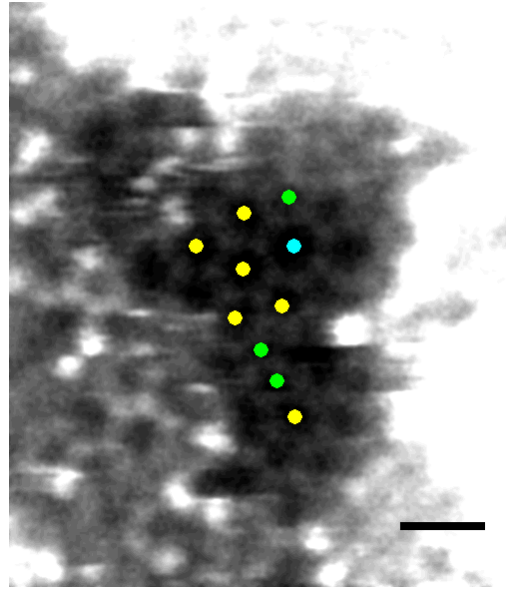


Figure A.26

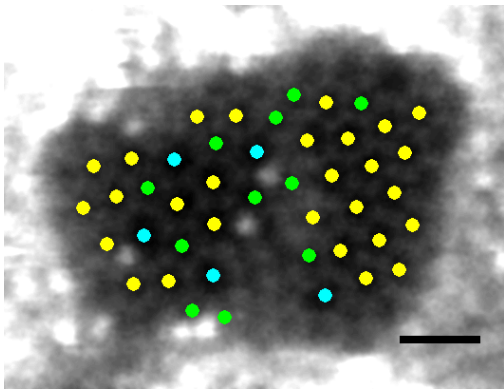


Figure A.27

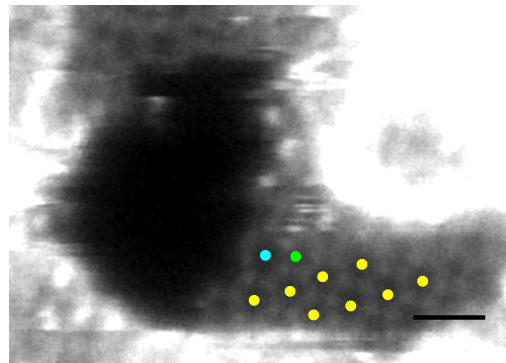


Figure A.28

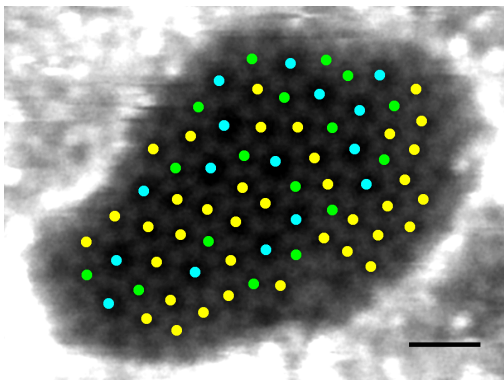


Figure A.29

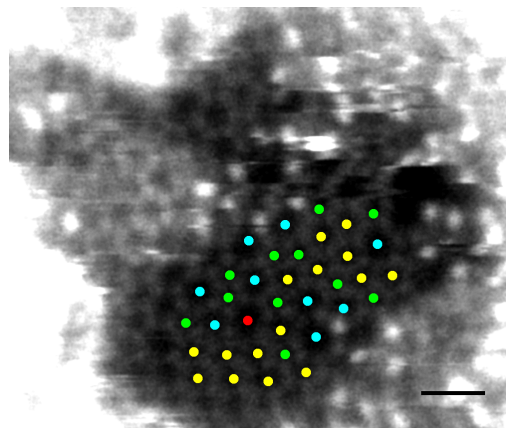


Figure A.30

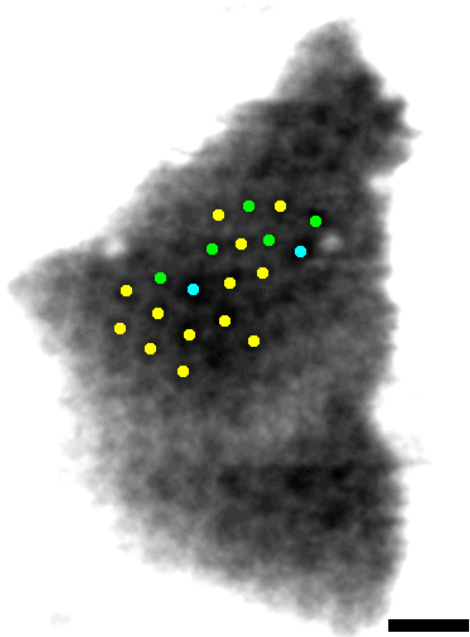


Figure A.31

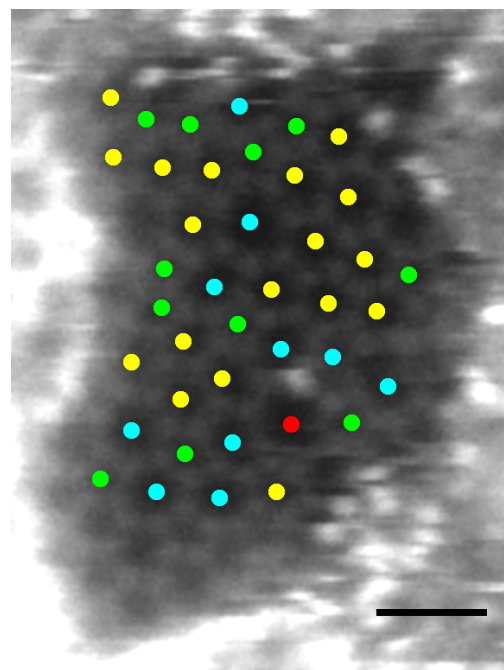


Figure A.32

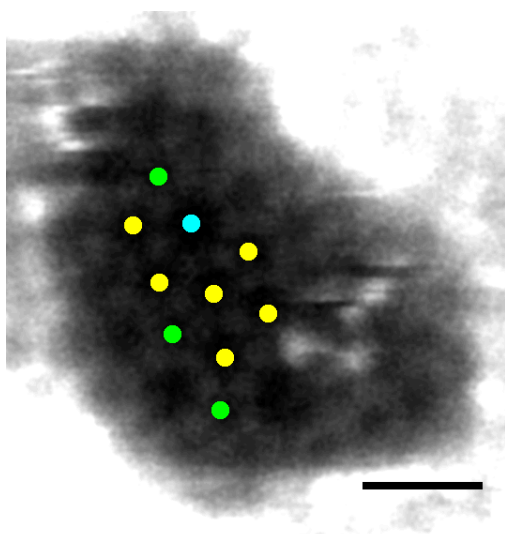


Figure A.33

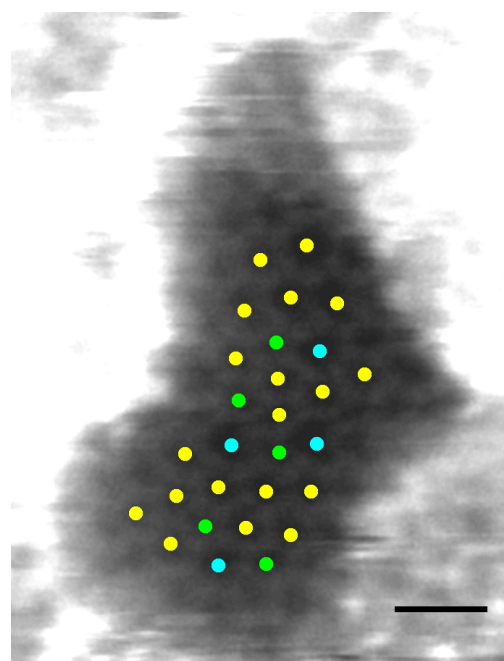


Figure A.34

List of Figures

2.1	Schematic layout of a TEM with extensions for energy dispersive X-ray spectroscopy and electron energy loss spectroscopy (taken from reference [10])	5
2.2	Ray path in a TEM between sample and screen of (A) the diffraction mode and (B) the imaging mode (taken from reference [14])	7
2.3	Illustration of the reciprocity principle in TEM and STEM (adapted from reference [16])	8
2.4	(a) Layout of a STEM containing the main components; (b) Photograph of the Nion STEM in Vienna used for the experiments in this thesis (taken from reference [5])	10
2.5	Schematic diagram of an AFM	11
2.6	a) Illustration of the used TEM-grids consisting of gold bars; b) diagram of one magnified gold square of the grid to illustrate the perforated carbon foil (taken from reference [5])	13
3.1	TEM image of a 1.4 nm thick sample showing a crack (0) and one (1), two (2), and three (3) layers of the carbon film.	16
3.2	TEM image of an edge in a 2.2 nm thick carbon film probably caused by a step in the salt surface	17
3.3	TEM image of an 0.5 nm thick carbon sample where the transfer was not successful, most of the grid was not covered with carbon, and just very few little carbon flakes could be found	17

3.4	Electron diffraction pattern of a 1.5 nm thick amorphous carbon film	18
3.5	Overlay of the diffraction pattern in fig. 3.4 and a diffraction pattern of pristine graphene to show the sp^2 -structure of the carbon film . . .	19
3.6	AFM image of an 0.8 nm thin carbon film showing single and double layers of the carbon film as well as holes in the film	21
3.7	Height profile along the red arrow in fig. 3.6	21
3.8	STEM image of an 0.8 nm thick carbon film showing an area of 384×384 nm with holes (black areas) and different thicknesses	23
3.9	STEM image of an 0.8 nm thick carbon film showing an area of 96×96 nm with holes (black areas) and different thicknesses	23
3.10	STEM image of an 0.8 nm thick carbon film showing the inhomogeneous structure similar to the images in [7, 8]; the black areas represent holes in the film	24
3.11	STEM image of an 0.8 nm thick carbon film showing areas where the atomic structure of the two-dimensional film is visible	24
3.12	STEM image of an 0.8 nm thick carbon film showing the atomic structure of a single layer of the amorphous film	25
3.13	Steps in the process of image analysis for the ring statistics based on the image shown in fig. 3.12: a) atoms are marked with grey dots, b) polygons are identified in the model	26
3.14	STEM image of an 1.4 nm thick carbon film (left) and corresponding ring analysis (right)	26
3.15	STEM image of an 1.4 nm thick carbon film (left) and corresponding ring analysis (right)	27
3.16	STEM image of an 1.4 nm thick carbon film (left) and corresponding ring analysis (right)	27
3.17	STEM images of a sample by Andrey Turchanin consisting of disordered membranes created via annealing of organic molecules	30

Bibliography

- [1] W. H. Zachariasen, “The atomic arrangement in glass,” *Journal of the American Chemical Society*, vol. 54, no. 10, pp. 3841–3851, 1932.
- [2] A. C. Wright, “Neutron scattering from vitreous silica. v. the structure of vitreous silica: What have we learned from 60 years of diffraction studies?” *Journal of Non-Crystalline Solids*, vol. 179, no. 0, pp. 84 – 115, 1994, proceedings of the First {PAC} {RIM} Meeting on Glass and Optical Materials.
- [3] P. Y. Huang, S. Kurasch, A. Srivastava, V. Skakalova, J. Kotakoski, A. V. Krasheninnikov, R. Hovden, Q. Mao, J. C. Meyer, J. Smet, D. A. Muller, and U. Kaiser, “Direct imaging of a two-dimensional silica glass on graphene,” *Nano Letters*, vol. 12, no. 2, pp. 1081–1086, 2012.
- [4] L. Lichtenstein, M. Heyde, and H.-J. Freund, “Crystalline-vitreous interface in two dimensional silica,” *Physical Review Letters*, vol. 109, p. 106101, Sep 2012.
- [5] F. Eder, “A microscopic analysis of deliberately introduced structural modifications in free-standing graphene,” Ph.D. dissertation, Univerity of Vienna, 2014.
- [6] J. Kotakoski, A. V. Krasheninnikov, U. Kaiser, and J. C. Meyer, “From point defects in graphene to two-dimensional amorphous carbon,” *Physical Review Letters*, vol. 106, p. 105505, Mar 2011.
- [7] M. Isaacson, M. Ohtsuki, and M. Utlaut, “Can we determine the structure of thin amorphous films using scanning transmission electron microscopy?” *Proceedings of the 37th Annual EMSA Meeting*, pp. 498–501, 1979.
- [8] M. S. Isaacson, “Seeing single atoms,” *Ultramicroscopy*, vol. 123, no. 0, pp. 3–12, 2012, albert Victor Crewe Memorial Issue.
- [9] M. Knoll and E. Ruska, “Das Elektronenmikroskop,” *Zeitschrift für Physik*, vol. 78, pp. 318–339, 1932.

- [10] L. Reimer and H. Kohl, *Transmission Electron Microscopy: Physics of Image Formation*, ser. Springer Series in Optical Sciences. Springer, 2008.
- [11] M. De Graef, *Introduction to Conventional Transmission Electron Microscopy*. Cambridge University Press, 2003.
- [12] J. C. Meyer, C. Kisielowski, R. Erni, M. D. Rossell, M. F. Crommie, and A. Zettl, “Direct imaging of lattice atoms and topological defects in graphene membranes,” *Nano Letters*, vol. 8, no. 11, pp. 3582–3586, 2008.
- [13] Delong America. [Online]. Available: <http://www.lv-em.com/>
- [14] D. Williams and C. Carter, *Transmission Electron Microscopy: A Textbook for Materials Science*, ser. Cambridge library collection. Springer, 2009.
- [15] A. V. Crewe, “A new kind of scanning microscope,” *Journal de Microscopie*, vol. 2, pp. 369–371, 1963.
- [16] S. Pennycook, A. Lupini, M. Varela, A. Borisevich, Y. Peng, M. Oxley, K. Van Benthem, and M. Chisholm, “Scanning transmission electron microscopy for nanostructure characterization,” in *Scanning Microscopy for Nanotechnology*, W. Zhou and Z. L. Wang, Eds. Springer New York, 2007, pp. 152–191.
- [17] O. L. Krivanek, N. Dellby, A. A. Spence, R. A. Camps, and L. M. Brown, “Aberration correction in the STEM,” in *Electron Microscopy and Analysis 1997*, ser. Institute of Physics Conference Series, J. M. Rodenburg, Ed., no. 153. IOP Publishing Ltd, 1997, pp. 35–40.
- [18] Nion. [Online]. Available: <http://www.nion.com/>
- [19] O. L. Krivanek, G. J. Corbin, N. Dellby, B. F. Elston, R. J. Keyse, M. F. Murfitt, C. S. Own, Z. S. Szilagy, and J. W. Woodruff, “An electron microscope for the aberration-corrected era,” *Ultramicroscopy*, vol. 108, no. 3, pp. 179–195, 2008.
- [20] G. Binnig, C. F. Quate, and C. Gerber, “Atomic force microscope,” *Physical Review Letters*, vol. 56, pp. 930–933, 1986.
- [21] R. García and R. Pérez, “Dynamic atomic force microscopy methods,” *Surface Science Reports*, vol. 47, no. 6–8, pp. 197–301, 2002.
- [22] Park Systems. [Online]. Available: <http://www.parkafm.com/>

- [23] Leica Microsystems. [Online]. Available: <http://www.leica-microsystems.com/>
- [24] Quantifoil Micro Tools GmbH. [Online]. Available: <http://www.quantifoil.com/>
- [25] J. C. Meyer, C. O. Girit, M. F. Crommie, and A. Zettl, “Hydrocarbon lithography on graphene membranes,” *Applied Physics Letters*, vol. 92, no. 12, p. 123110, 2008.
- [26] J. Robertson and E. P. O’Reilly, “Electronic and atomic structure of amorphous carbon,” *Physical Review B*, vol. 35, pp. 2946–2957, 1987.
- [27] J. Robertson, “Diamond-like amorphous carbon,” *Materials Science and Engineering: R: Reports*, vol. 37, no. 4–6, pp. 129–281, 2002.
- [28] J. Kakinoki, Y. Komura, and T. Ino, “Electron diffraction study of evaporated carbon films,” *Acta Crystallographica*, vol. 13, no. 3, pp. 171–179, 1960.
- [29] A. Turchanin, D. Weber, M. Bünenfeld, C. Kisielowski, M. V. Fistul, K. B. Efetov, T. Weimann, R. Stosch, J. Mayer, and A. Götzhäuser, “Conversion of self-assembled monolayers into nanocrystalline graphene: Structure and electric transport,” *ACS Nano*, vol. 5, no. 5, pp. 3896–3904, 2011.

David Lindner

Curriculum Vitae

Personal Data

Date of Birth 12.04.1989
Place of Birth Bozen (Italy)
Nationality Italian

Education

10/2011 – present **Bachelor Studies in Mathematics**, *University of Vienna*.
03/2013 – 06/2015 **Master Studies in Physics**, *University of Vienna*.
10/2009 – 03/2013 **Bachelor Studies in Physics**, *University of Vienna*.
09/2003 – 07/2009 **High School**, *Franziskanergymnasium Bozen*.

Language Skills

German native
English fluent
Italian fluent

Computer Skills

Programming MATLAB, Mathematica, VBA
Microsoft Office Word, Excel, PowerPoint, Outlook, Visio, Publisher
Text Processing \LaTeX